HHS Public Access

Author manuscript

Cell Rep. Author manuscript; available in PMC 2021 December 23.

Published in final edited form as:

Cell Rep. 2021 November 09; 37(6): 109978. doi:10.1016/j.celrep.2021.109978.

Disrupted population coding in the prefrontal cortex underlies pain aversion

Anna Li[1,2,6], **Yaling Liu**[1,6], **Qiaosheng Zhang**[1,2], **Isabel Friesner**[1,2], **Hyun Jung Jee**[1,2], **Zhe Sage Chen**[2,3,4,5], **Jing Wang**[1,2,3,5,7,*]

[1]Department of Anesthesiology, Perioperative Care and Pain Medicine, New York University Grossman School of Medicine, New York, NY, USA

[2]Interdisciplinary Pain Research Program, New York University Langone Health, New York, NY, USA

[3]Department of Neuroscience and Physiology, New York University School of Medicine, New York, NY, USA

[4]Department of Psychiatry, New York University School of Medicine, New York, NY, USA

[5]Neuroscience Institute, New York University School of Medicine, New York, NY, USA

[6]These authors contributed equally

[7]Lead contact

SUMMARY

The prefrontal cortex (PFC) regulates a wide range of sensory experiences. Chronic pain is known to impair normal neural response, leading to enhanced aversion. However, it remains unknown how nociceptive responses in the cortex are processed at the population level and whether such processes are disrupted by chronic pain. Using *in vivo* endoscopic calcium imaging, we identify increased population activity in response to noxious stimuli and stable patterns of functional connectivity among neurons in the prelimbic (PL) PFC from freely behaving rats. Inflammatory pain disrupts functional connectivity of PFC neurons and reduces the overall nociceptive response. Interestingly, ketamine, a well-known neuromodulator, restores the functional connectivity among PL-PFC neurons in the inflammatory pain model to produce anti-aversive effects. These results suggest a dynamic resource allocation mechanism in the prefrontal representations of pain and indicate that population activity in the PFC critically regulates pain and serves as an important therapeutic target.

*Correspondence: jing.wang2@nyumc.org.

AUTHOR CONTRIBUTIONS

A.L., Y.L., and H.J.J. performed the behavior experiments. A.L., Y.L., H.J.J., and Q.Z. performed the *in vivo* calcium imaging experiments. A.L., Q.Z., I.F., and Z.S.C. analyzed data. J.W. designed all the experiments and supervised the study with assistance from Z.S.C. J.W. wrote the manuscript with help from other authors.

SUPPLEMENTAL INFORMATION

Supplemental information can be found online at https://doi.org/10.1016/j.celrep.2021.109978.

DECLARATION OF INTERESTS

The authors declare no competing interests.

Graphical Abstract

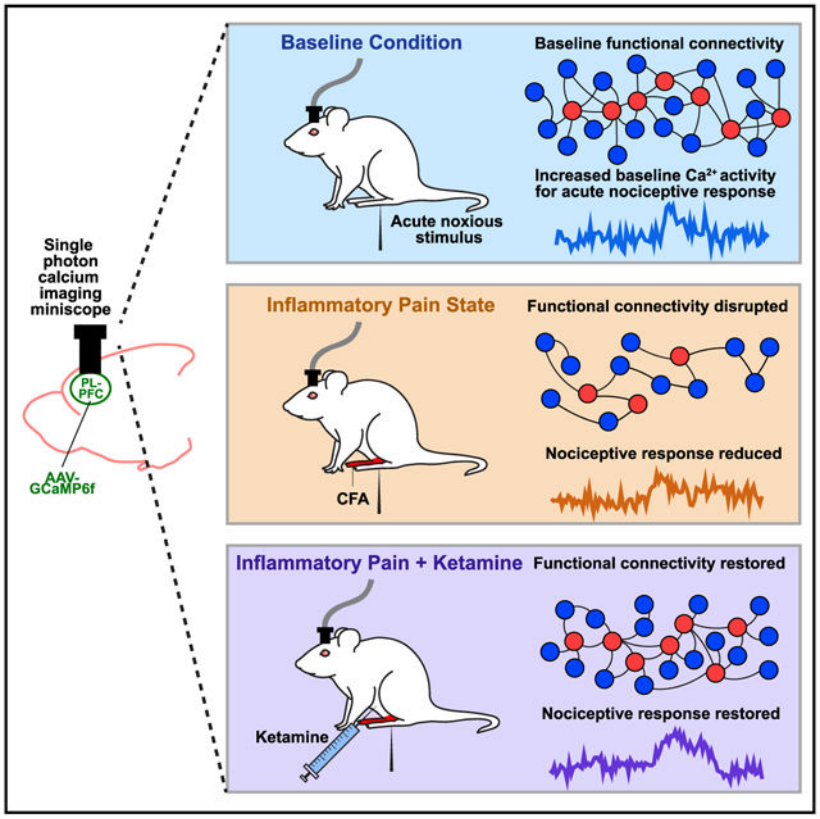

In brief

Li et al. reveal that inflammatory pain disrupts the functional connectivity of neurons in the prelimbic prefrontal cortex (PL-PFC) and the overall nociceptive response. Ketamine, meanwhile, restores the functional connectivity of neurons in the PL-PFC in the inflammatory pain state to produce anti-aversive effects.

INTRODUCTION

Neural responses to noxious inputs prevent us from injury (Basbaum et al., 2009). One such response is aversion, which produces a learning signal to avoid potentially harmful situations. Chronic pain, meanwhile, is known to impair the endogenous response to noxious inputs, resulting in enhanced pain aversion (Radzicki et al., 2017; Ren et al., 2021; Zhang et al., 2017). Given the role the cerebral cortex plays in aversion-type behaviors, including pain-aversive behaviors (Cheriyan and Sheets, 2018; Dale et al., 2018; Huang et al., 2019; Johansen and Fields, 2004; Navratilova et al., 2015; Rainville et al., 1997; Zhang et al., 2015, 2017), detailed circuit-level mechanisms of cortical processing provide a key to our understanding of pain.

The prefrontal cortex (PFC) integrates sensory inputs and in turn provides both top-down and cortico-cortical regulation of such inputs (Salzman and Fusi, 2010). Recent studies

indicate that neurons in the PFC can increase their firing rates in response to noxious stimuli, but such response is diminished by the presence of chronic pain (Dale et al., 2018; Ji and Neugebauer, 2011; Kelly et al., 2016; Radzicki et al., 2017; Talay et al., 2021; Zhang et al., 2015). *In vitro* studies in rodent models have further demonstrated decreased excitability of pyramidal neurons in the PFC under chronic pain conditions (Ji and Neugebauer, 2011; Kelly et al., 2016; Radzicki et al., 2017; Zhang et al., 2015). What remains unknown, however, is how pain information is encoded and processed in the PFC at the population level in freely behaving animals, and how chronic pain impairs population-level pain processing.

In subcortical areas, pain-specific neurons have been identified that produce direct regulatory outputs (Corder et al., 2019; Craig et al., 1994). However, it is unclear whether such exclusively pain-specific neurons exist in the PFC to consistently respond to noxious stimuli. An alternative to cell-specific processing is population coding. Studies have shown that cortical neurons are capable of conjunctive tuning, where the computational output of neural ensembles, rather than fixed synaptic outputs of individual neurons, provides the basis for the performance of certain cognitive tasks (Fusi et al., 2016; Ramirez-Cardenas and Viswanathan, 2016; Rigotti et al., 2013). In this model, each neuron is capable of serving multiple functions and is recruited into a specific functional neural circuit in a particular behavioral context. This model is compatible with the principle of dynamic resource allocation, where biological resources are allocated dynamically according to the computing load or cognitive demand (Alonso et al., 2014; Bays and Husain, 2008; Bruning and Lewis-Peacock, 2020; Yoo et al., 2018). This coding principle allows cortical neurons to perform multiple cognitive tasks in a flexible and efficient manner. However, it is not known whether such coding scheme based on population activity is utilized by the cortex, specifically the PFC, to process and regulate pain, and if so, how this scheme is impaired by chronic pain.

Functional connectivity between groups of neurons provides understanding of population-level neural responses to sensory inputs, and it has been used to characterize pain and other neuropsychiatric disorders based on various modalities of neural recording techniques, such as microcircuit-level calcium imaging (Cramer et al., 2019) and brain-wide neuroimaging (Baliki et al., 2012; Kano et al., 2020; Mutso et al., 2012; Spisak et al., 2020). Functional connectivity analyses have successfully identified long-range nociceptive information flow within the brain in chronic pain conditions (Baliki et al., 2012; Vachon-Presseau et al., 2019), thereby having the potential to provide insight into population neural responses within a specific cortical area as well. The recent development of graph-theoretic approaches enables detailed functional connectivity analysis of local networks, further facilitating studies of high-order population coding within specific cortical areas such as the PFC (Bonifazi and Massobrio, 2019; Sporns, 2018).

Ketamine is an important pharmacological neuromodulator used to treat a number of neuropsychiatric diseases including chronic pain (Doan and Wang, 2018; Machado-Vieira et al., 2009; Maeng et al., 2008). Studies have shown that it can produce long-lasting mood-elevating effects (Machado-Vieira et al., 2009), by inhibiting N-methyl-D-aspartate (NMDA) receptors and by promoting the translation of synaptic proteins (Autry et al., 2011;

Li et al., 2010). Recent studies also indicate that ketamine can produce similarly long-lasting anti-aversive effects (Wang et al., 2011), and it is emerging as an important pharmacological therapy for chronic pain (Cohen et al., 2018; Doan and Wang, 2018). However, analgesic mechanisms for ketamine in the brain are poorly understood. For example, it remains unknown how cellular and molecular effects of ketamine translate to the reshaping of cortical circuits, especially in the chronic pain condition, to regulate aversion.

In this study, we measured *in vivo* calcium activity in pyramidal neurons of the prelimbic (PL) region of the PFC (PL-PFC) in awake, freely behaving rats to examine prefrontal processing of nociceptive information. We found that a significant number of these PFC neurons increased their activity in response to noxious stimuli. Interestingly, we did not find neurons that specifically responded to acute pain signals on a consistent basis over time. Instead, we found consistent population-level changes in the PL-PFC, manifested by enhanced average firing rates in response to noxious stimuli, as well as by stable resting-state functional connectivity between pain-responsive neurons and other neurons. Inflammatory pain, however, decreased the population firing response to nociceptive inputs, and reduced inter-neuronal communication within the PL-PFC. Meanwhile, ketamine restored the endogenous population activity in the PL-PFC and decreased pain aversion. Optogenetic inactivation of the pyramidal neurons in the PL-PFC, however, removed the anti-aversive effects of ketamine. These results suggest that population activity in the PL-PFC at baseline and in response to nociceptive inputs is critical for endogenous pain control, and its impairment in chronic pain conditions may lead to enhanced aversion. These cortical mechanisms also form important therapeutic targets for neuromodulatory agents such as ketamine.

RESULTS

Inflammatory pain inhibits population-level nociceptive response in the PL-PFC

To measure the neural response in the PL-PFC, we injected GCaMP6f into the PL-PFC. GCaMP6f was used as a readout for neural activity and was not expressed in a projection-specific manner. We used a head-mounted endoscopic microscope with a 1.0 mm diameter × ~9.0 mm length lens to track the Ca^{2+} activity in the soma of pyramidal neurons that expressed CaMKII (Figures 1A, 1B, and S1A). We measured Ca^{2+} activity before and after a noxious mechanical stimulus (27G pin prick [PP]) or a control, non-noxious (0.4 g von Frey filament [vF]) stimulus in the contralateral paw of awake, freely behaving rats (Figures 1A, 1B, and S1B). After signal processing and identification of active cells (Figures 1C–1E), we found that PL-PFC neurons exhibited only low-level Ca^{2+} activity in response to the non-noxious stimulus (Figures 1F and 1G); in contrast, these neurons exhibited an increase in Ca^{2+} activity in response to the noxious stimulus (Figures 1F and 1H). We then examined the average peak ΔF of Ca^{2+} activity in response to both non-noxious and noxious stimuli and found that peak fluorescence was significantly higher in response to noxious stimuli than non-noxious stimuli (Figure 1I). These results are compatible with previous findings that suggest neurons in the PFC increase their firing rates in response to noxious stimuli (Dale et al., 2018; Talay et al., 2021). Furthermore, the number of neurons that responded to the noxious stimulus was greater than the number of neurons responsive to

the non-noxious stimulus (Figures 1J–1L). These results raised the question whether a select group of neurons in the PL-PFC could respond specifically and consistently to nociceptive inputs. Because such specificity is expected to be preserved over time, we then compared Ca^{2+} activity in response to noxious stimuli across recording sessions on different days. Here, we found that very few neurons actually consistently responded to noxious stimuli across different recording sessions (Figures S2A–S2C). In contrast, the average peak ΔF response for all the PL-PFC neurons was well preserved over time (Figure S2D). These results suggest that nociceptive inputs are processed not necessarily at the level of individual pain-specific neurons, but rather at the population level in the PL-PFC.

We then investigated how this population-level nociceptive response in PL-PFC is affected by the presence of inflammatory pain. Previous studies have shown that chronic pain induces anatomically non-specific enhancement in pain aversion and associated cortical maladaptive plasticity (Dale et al., 2018; Zhang et al., 2017; Zhou et al., 2018a). Thus, we injected complete Freund's adjuvant (CFA) into the hind paw ipsilateral to lens implant to model inflammatory pain and performed peripheral stimulations in the paw opposite to CFA injection to avoid confounding spinal and peripheral hypersensitivity (Figure 1M). We found that CFA-treated rats exhibited substantially decreased Ca^{2+} activity in response to noxious stimuli (Figures 1N–1P and S3). The proportion of pain-responsive neurons recorded in the PL-PFC of CFA-treated rats also decreased accordingly (Figures 1Q and 1R). In contrast, inflammatory pain did not significantly alter the cortical response to non-noxious stimuli when they are applied to uninjured paws (Figure S4). These results support the importance of PL-PFC neurons in pain processing and suggest deficits in PL-PFC population activity as a potential mechanism for chronic pain.

Ketamine increases the nociceptive response at the population-level in the PL-PFC

Ketamine is known to produce long-lasting relief of the affective component of pain and thus has the potential to be an important pharmacological neuromodulation therapy for chronic pain (Cohen et al., 2018; Doan and Wang, 2018). Previous studies have suggested the PFC to be a target for ketamine in mood regulation (Li et al., 2010), and hence we investigated whether restoration of the population nociceptive response in the PL-PFC constitutes an important analgesic mechanism for ketamine in the inflammatory pain model. We administered an intraperitoneal sub-anesthetic (10 mg/kg) dose of ketamine to CFA-treated rats, based on previous studies (Wang et al., 2011) (Figures 2A and 2B). Ketamine is known to have short-lived anti-nociceptive effects, manifested by temporary relief of sensory allodynia (Figure 2C). Interestingly, we found that days after the administration of ketamine, long after the transient relief of allodynia has disappeared, PL-PFC pyramidal neurons continued to demonstrate an increase in the average peak ΔF in response to noxious stimuli (Figures 2D–2F). This persistent increase in cortical nociceptive response was not observed in rats that received an injection of saline control (Figures 2D, 2G, and 2H). These results indicate that a single dose of ketamine could produce long-lasting restoration of the population nociceptive response of PL-PFC neurons in the inflammatory pain state.

Resting-state functional connectivity in the PL-PFC is impaired in the inflammatory pain model but restored by ketamine

Our data indicate that average neural response in the PL-PFC to nociceptive inputs declines in the inflammatory pain condition, whereas ketamine restores such response. To understand the underlying mechanism for such population response, we applied the graph-theoretic functional connectivity analysis to examine the relationship between neurons in a given brain region, and how such relationship is altered by inflammatory pain and repaired by ketamine. Specifically, we first normalized the time-series Ca^{2+} fluorescence data and applied fast nonnegative spike deconvolution method to infer the relative spiking activities from preprocessed Ca^{2+} activities of individual PFC neurons (Figure 3A) (Friedrich et al., 2017). These proxy spiking activities allowed us to assess the scale-invariant cross-correlation between PFC neurons. In order to quantitatively compare functional connectivity between PFC neurons during baseline, CFA, and post-ketamine conditions, we subsampled proportionally a subset of pain-responsive and nonresponsive neurons for each given rat (Figure 3B; STAR Methods). First, we calculated cumulative distribution functions for all the pain-responsive or nonresponsive neurons, ordered by each neuron's basal firing rate (Figure 3B left). We then determined the numbers of subsampled pain-responsive and nonresponsive neurons based on the number of pain-responsive neurons and total number of neurons across all sessions for each rat. Finally, based on the cumulative distribution function, we selected a subsample of neurons to ensure a uniform distribution of firing rates among sampled pain-responsive and nonresponsive neurons (Figure 3B).

Next, we calculated betweenness centrality (C_B) and degree centrality (C_D) as graph-network statistics to evaluate the importance of pain-responsive neurons in the flow of nociceptive information within pyramidal neurons of the PL-PFC. Within the PL-PFC network, individual neurons were treated as nodes. In the graph theory, betweenness centrality is a measure of the volume of shortest paths that pass through a given node (De Vico Fallani et al., 2014; Kwon et al., 2019), which provides insight into the importance of that node (as a hub) in the passage of information throughout the overall neural network (Figure 4A). Meanwhile, degree centrality is a measure of the number of edges attached to a given node (De Vico Fallani et al., 2014; Kwon et al., 2019), which indicates the level of connectivity of this node as a functional hub to other nodes within the entire network (Figure 4B). Therefore, these two network statistics provide insight into how pain-responsive or nonresponsive neurons connect with other neurons within the PL-PFC to process nociceptive information.

We found that pain-responsive neurons as functional hubs demonstrated stable betweenness centrality across time in the baseline condition (Figure S5A). Likewise, pain-nonresponsive neurons also demonstrated stable betweenness centrality (Figure S5B). Similar stability was observed for degree centrality as well (Figures S5C and S5D). These results indicate that functional connectivity between subsampled neurons in the PL-PFC was relatively stable at baseline. This consistency of resting-state functional connectivity measures among pain-responsive neurons is compatible with the consistent average Ca^{2+} response among neurons in the PL-PFC in the presence of noxious stimuli (Figure S2D). This is in contrast to the lack of consistency in the identification of individual pain-responsive neurons (Figures

S2A–S2C). These results suggest that although the identity of individual pain-responsive neurons may change over time, the functional connections between pain-responsive neurons and other neurons remain relatively constant to maintain a stable network response to nociceptive inputs at baseline. In contrast, we observed a significant decrease in the betweenness centrality of pain-responsive neurons after CFA treatment (Figures 4C and 4D), suggesting a reduced information flow traffic between pain-responsive nodes as functional hubs and the other nodes. Interestingly, nonresponsive neurons did not show such a decline (Figure 4E). These results suggest that inflammatory pain specifically impairs functional connectivity between pain-responsive neurons and other neurons within the PL-PFC, and thus diminishing the network roles for these pain-responsive neurons as functional information hubs. Ketamine, meanwhile, increased betweenness centrality in CFA-treated rats and restored this measure back to the baseline condition (Figures 4C and 4D). Similar decline was observed in degree centrality among pain-responsive neurons in CFA-treated rats, and ketamine also repaired this defect (Figures 4F–4H). Finally, we did not observe such therapeutic effects on functional connectivity in CFA rats that received saline (control) treatment (Figure S6). Together, these results indicate that the presence of inflammatory pain specifically reduces functional connectivity between pain-responsive neurons and the remaining neurons within the PFC network, thereby minimizing the flow of information that passes through these neurons in the PL-PFC. The restoration of the functional connectivity between pain-responsive neurons and other neurons within the PL-PFC, meanwhile, constitutes an important circuit mechanism for ketamine.

Ketamine provides long-lasting inhibition of pain aversion

Given this ability of ketamine to repair functional connectivity within the PL-PFC in the inflammatory pain model, we investigated the role of PL-PFC in mediating the anti-aversive function of ketamine, using a conditioned place aversion (CPA) assay (Figures 5A and 5B), a classic test to assess pain aversion in rodent models (Johansen et al., 2001; King et al., 2009; Martinez et al., 2017; Singh et al., 2020; Zhang et al., 2017). During the preconditioning phase, rats were allowed to move freely between two chambers. During the conditioning phase, one of the chambers was paired with repeated noxious stimulation (PP) of the hind paw, whereas the opposite chamber was not paired with PP. During the testing phase, rats were once again allowed to move freely between two chambers without peripheral stimuli. Here, we found that although rats in general demonstrated an aversion to noxious stimuli, as shown by avoidance of the chamber paired with PP (Figure 5C), rats with inflammatory pain (after CFA injections) showed further increased pain aversion (Figure 5D). Pain aversion can be quantitated by a CPA score, which is calculated by subtracting the time rats stayed in the PP-paired chamber during the testing phase from the time they spent in that chamber during the preconditioning phase. A higher CPA score indicates greater pain aversion, and CFA-treated rats showed higher CPA scores (Figure 5E), indicating that the presence of inflammatory pain enhances the aversive value of acute noxious inputs, compatible with previous results (Dale et al., 2018; Singh et al., 2020; Zhang et al., 2017).

We then assessed the aversive symptoms of CFA-treated rats after ketamine administration. To avoid confounding anti-nociceptive effects, we waited for the resolution of these anti-nociceptive effects to perform the CPA assays. We found that 2 days after a single dose

of ketamine, CFA-treated rats demonstrated a substantially decreased aversive response to noxious stimuli, as shown by a lack of avoidance of the PP-paired chamber and a lower CPA score (Figures 5F–5H). This anti-aversive effect was substantially greater in CFA-treated than saline-treated rats, suggesting an increased impact of ketamine on inflammatory pain (Figure S7). In contrast, CFA-treated rats that received saline (control) treatment did not demonstrate this decrease (Figures 5F–5H). We repeated these CPA tests 5 days after ketamine and found similar results (Figures 5I–5K). These data indicate that ketamine produced long-lasting relief of pain aversion.

PL-PFC mediates the anti-aversive effects of ketamine

Next, we investigated whether restoration of the population response in the PL-PFC mediates the anti-aversive effects of ketamine. We used an optogenetic strategy to inactivate pyramidal neurons to inhibit basal activities and thus resting-state functional connectivity within the PL-PFC. We introduced halorhodopsin (NpHR) via a CaMKII promoter in the PL-PFC and used a laser to activate NpHR to specifically target pyramidal neurons that expressed these receptors (Figure 6A). During conditioning, we paired one chamber with PL-PFC inactivation and noxious stimulation (PP), and other chamber without either cortical neuromodulation or peripheral stimulation in CFA-treated rats (Figure 6B). We found that in control rats that expressed YFP, ketamine was able to reduce pain aversion, as shown by the reduction of avoidance of PP-paired chamber (Figure 6C). However, when we paired PL-PFC inactivation with PP, it removed the anti-aversive effects of ketamine, as shown by avoidance of the PP chamber (Figures 6D and 6E). These results of causal manipulation indicate that population activity in the PL-PFC plays a critical role in regulating pain-aversive behaviors and that its inhibition removed the anti-aversive effects of ketamine.

To further validate these findings, we tested whether pharmacological activation of the PL-PFC with agents sharing molecular properties of ketamine could reproduce the anti-aversive effects of systemic administration of ketamine. Ketamine is known to block N-methyl-D-aspartate (NMDA) receptors to modify cortical synaptic plasticity (Autry et al., 2011; Li et al., 2010). Thus, we injected AP5, a selective blocker of NMDA receptors, in the PL-PFC of CFA-treated rats and then performed CPA assays to assess pain aversion (Figures 7A–7C and S8). We found that rats that received AP5 treatment did not demonstrate an avoidance of the PP-paired chamber, in contrast to saline-treated (control) rats (Figures 7D–7F). These results mirror findings from intraperitoneal ketamine injections, suggesting that NMDA blockade in the PL-PFC likely mediates the anti-aversive effects of ketamine.

Previous studies in the field of depression showed that NMDA receptor blockade mediated by ketamine induces the activation of mammalian target of rapamycin complex 1 (mTORC1), a key translational regulator (Li et al., 2010; Zhou et al., 2014). mTORC1 activation, in turn, increases local translation of synaptic proteins in the cortex (Li et al., 2010; Zhou et al., 2014). Thus, we studied the role of mTORC1 in the PL-PFC in mediating the anti-aversive effect of ketamine. Before ketamine administration, rapamycin, a specific blocker of mTORC1, was injected into the PL-PFC. We then performed CPA assays to assess pain aversion (Figures 7G and 7H). We found that rapamycin blocked the anti-aversive effect of ketamine (Figures 7I–7K). These results indicate that mTORC1 is

involved in ketamine's inhibition of aversive pain symptoms. Together, these behavioral data indicate that the PL-PFC is likely an important target for the anti-aversive effects of ketamine.

DISCUSSION

In this study, we found that neurons in the PFC respond to noxious stimuli in a population-specific manner. Although the exact role of individual neurons can shift over time, the population activity in the PL-PFC remains consistent both at baseline and in response to pain stimuli, as manifested by stable patterns of functional connectivity and increased average Ca^{2+} response. Whereas inflammatory pain disrupts the functional connectivity within the PL-PFC, leading to impaired population response, ketamine restores it to produce anti-aversive effects.

In the pain field, functional connectivity analysis has been used to investigate information flow across large regions in the brain (Baliki et al., 2012; Vachon-Presseau et al., 2019). Our study here applies the graph-theory approach to analyze functional connectivity among neurons within a single cortical region. In the graph theory, betweenness centrality is a measure of centrality in a graph based on the shortest path. This measure defines the connectivity within a network, where high betweenness indicates the potential to dissociate network connections when a given node is removed. Meanwhile, degree centrality is a measure of how centrally connected a given node is to other nodes within the entire neural network (De Vico Fallani et al., 2014; Kwon et al., 2019). These two network statistics focus on identifyingneurons that act as hubs for organizing information flow in a network, and they have been proven to be valuable tools for understanding the circuit mechanisms of a number of neurological conditions (Bilbao et al., 2018; Komaki et al., 2016; Minati et al., 2013; Redcay et al., 2013). We found that nodes—neurons—that are pain-responsive demonstrate high betweenness centrality and degree centrality and thus serve as hubs of communication to other neurons. In other words, although the identity of the pain-specific neurons may shift over time, neurons that respond to noxious inputs at any given moment can coordinate a similar network response within the PFC to regulate pain. Thus, pain responsiveness is preserved at the network level, rather than at the level of individual neurons. As shown in numerous prior studies, a stable pattern in resting-state functional connectivity among PFC neurons can in turn drive the nociceptive response (Baliki et al., 2012; Vachon-Presseau et al., 2019). The impairment of even a subpopulation of PFC neurons, meanwhile, has the potential to substantially disrupt the overall prefrontal pain network. Thus, this population-coding mechanism also provides a conceptual link between *in vitro* cellular findings that showed decreased excitability of certain pyramidal neurons in the PFC (Ji and Neugebauer, 2011; Kelly et al., 2016; Radzicki et al., 2017; Zhang et al., 2015) and *in vivo* findings of decreased overall PFC function in the chronic pain condition (Apkarian et al., 2004; Dale et al., 2018; Geha et al., 2008; Moayedi et al., 2011).

Unlike other sensory experiences such as vision and hearing, there is no primary pain cortex. Instead, a distributed network of cortical circuits regulates pain. As a result, it is unclear whether the cortex, particularly cortical areas such as the PFC that do not directly receive and preprocess sensory information, has pain-specific neurons. Although our results

do not preclude the possibility that pain-specific neurons can be found in the PFC, they suggest that even if such neurons exist, they are likely sparsely distributed functionally. In subcortical areas such as the thalamus and amygdala, pain-specific neurons have been found to process sensory and/or affective information (Corder et al., 2019; Craig et al., 1994). Instead of cell-specific activity, our results here—consistent population nociceptive response and stable functional connectivity between pain-responsive neurons and other neurons—suggest that population-specific activity that is task-focused likely represents a dominant mechanism for pain processing in the PFC. As an executive control center, the PFC is known to respond to a large range of sensory and affective inputs to produce central commands to guide behavior. Therefore, our results are compatible with a dynamic resource-allocation mechanism, whereby individual neurons are recruited into a specific functional neural circuit in a particular context to encode and regulate behaviors. This population-based coding mechanism relies on population dynamics, rather than neurons with individually fixed, unique functions, to achieve regulatory functions of the PFC. This mechanism allows PFC neurons to perform multiple tasks in a flexible and efficient manner, including pain perception and regulation. This coding mechanism within the PFC has also been suggested in other cognitive functions such as working memory (Kobak et al., 2016; Markowitz et al., 2015; Murray et al., 2017). This population-specific nociceptive response has also recently been found in the anterior cingulate cortex (ACC), an area that is adjacent to the rodent prelimbic PFC but is known to enhance pain aversion (Acuña et al., 2020).

Ketamine has been shown to produce up to 2 weeks of mood improvement (Berman et al., 2000; Zarate et al., 2006). This is in contrast to the relatively short half-life of the anti-nociceptive effects this drug produces (Doan and Wang, 2018). This distinction may be particularly relevant to chronic pain conditions such as fibromyalgia, in which patients report chronic magnified emotional responses to wide-spread albeit sometimes low-intensity nociceptive inputs (Petzke et al., 2003; Scudds et al., 1987). Our results here suggest that ketamine may have a unique role in treating the affective component of chronic pain. One potential mechanism for such long-lasting effects is that inhibition of NMDA receptors can activate mTORC1 to promote local translation of synaptic proteins in the PFC (Li et al., 2010; Yang et al., 2013; Zhou et al., 2014). Our behavioral findings here indicate that through these similar cellular and molecular mechanisms, ketamine can enhance the activity of PFC neurons to reduce pain aversion. Just as importantly, our results also show that ketamine can restore functional connectivity and population activity in response to noxious inputs in the PL-PFC. This ability to reorganize functional connectivity within the PFC may be an important mechanism for ketamine in treating pain aversion as well as a number of other neuropsychiatric conditions. Interestingly, a previous study showed that ketamine decreased the hyperactivity of the ACC (Zhou et al., 2018a). In addition, ketamine can alter synaptic functions in the hippocampus through the expression of brain-derived neurotrophic factors (Autry et al., 2011; Garcia et al., 2008). Furthermore, the roles of NMDA receptors in the spinal cord have also been shown to contribute to the initiation and maintenance of chronic pain (Basbaum et al., 2009). Thus, ketamine can target a number of spinal and supraspinal regions either downstream or upstream to the PL-PFC, in concert to its modulation of prefrontal neurons, to impact pain behaviors. Future studies are therefore

needed to dissect neural circuits involving the PFC as well as other cortical and subcortical nodes to further define the mechanisms for the anti-aversive effects of ketamine.

In our study, we delivered GCaMP6f using a CaMKII promotor which primarily targeted pyramidal neurons. Although we cannot be absolutely certain that the Ca^{2+} activity we measured exclusively arose from pyramidal neurons, most of the recorded neurons likely comprised of pyramidal neurons. At the same time, interneurons are known to play a key role in regulating the excitability or plasticity of pyramidal neurons in the PFC (Zhang et al., 2015). Thus, there is a possibility that ketamine might also be able to block excitatory inputs into or plasticity of GABAergic interneurons, resulting in a reduced feed-forward inhibition of pyramidal neurons which, in turn, would increase the firing rates of excitatory output neurons. Future studies are needed to further dissect the roles of interneurons and pyramidal neurons to map out a more detailed functional pain network within the PFC and its modulation by ketamine. Furthermore, studies are also needed to elucidate the contribution of different cortical layers to pain processing and regulation.

Our results here do not exclude the possibility that pain-specific neurons can be found in other cortical areas such as the primary somatosensory cortex (S1). Indeed, the S1 is well-known to contribute to the sensory component of pain perception, and studies have indicated that neurons in certain areas of the S1 can play a critical role in discriminating nociceptive from non-nociceptive sensory inputs, and thus may carry pain-specific functions (Chen et al., 2009; Chudler et al., 1990; Kenshalo et al., 2000; Ploner et al., 2000; Tommerdahl et al., 1996; Whitsel et al., 2009, 2019). Future studies, including studies of functional connectivity, are needed to define the role of population activity in the S1 and other cortical areas in pain processing. Furthermore, imaging the effects of a broad range of stimuli across different cortical and subcortical regions could produce valuable information on the different pain coding schemes in the brain.

In summary, we have found that population-specific response in the PFC plays a critical role in pain regulation. Inflammatory pain disrupts the functional connectivity within the network of PFC neurons to impair endogenous nociceptive processing, whereas restoration of functional connectivity of PFC neurons likely contributes to the therapeutic mechanisms of ketamine.

STAR★METHODS

RESOURCE AVAILABILITY

Lead contact—Further information and requests for resources should be directed to and will be fulfilled by the Lead Contact, Jing Wang (jing.wang2@nyulangone.org).

Materials availability—This study did not generate new unique reagents.

Data and code availability

- All data reported in this paper will be shared by the lead contact upon request.

- All original code has been deposited at Zenodo and is publicly available as of the date of publication. DOIs are listed in the Key Resources Table.
- Any additional information required to reanalyze the data reported in this paper is available from the lead contact upon request.

EXPERIMENTAL MODEL AND SUBJECT DETAILS

Animals—All procedures were performed in accordance with the guidelines of New York University School of Medicine (NYUSOM) Institutional Animal Care and Use Committee (IACUC) to ensure minimal animal use and discomfort, as consistent with the NIH *Guide for the Care and Use of Laboratory Animals*. Sprague-Dawley male wild-type rats of the species *rattus norvegicus domestica* were purchased from Taconic Farms and pair-housed at the vivarium facility in the New York University Langone Science Building with controlled humidity, temperature, and 12 hr (6:30 AM-6:30 PM) light-dark cycle. Vendor health reports indicated that the rats were free of known viral, bacterial, and parasitic pathogens. All rats were purchased at a developmental stage of 7 weeks and given 10 days on average to adjust to the new environment before initiation of experiments. Rats with intracranial implants or injections were naive to procedures and drugs before surgical procedures.

METHOD DETAILS

Drugs—0.1 mL of Complete Freund's Adjuvant (CFA) (*Mycobacterium tuberculosis*, Sigma-Aldrich) was suspended in an oil:saline (1:2) emulsion and injected subcutaneously into the plantar aspect of the hind paw to induce inflammatory pain. CFA was injected contralateral to the paw that was stimulated by either pin prick (PP) or von Frey filament (vF). Ketamine hydrochloride (Ketaset) was purchased from Zoetis. Rats received 10 mg/kg ketamine injection intraperitoneally in the ketamine group, whereas a similar volume of saline was injected intraperitoneally to the control group. For intra prelimbic-prefrontal cortex (PL-PFC) injections, D-(−)-2-Amino-5-phos-phonopentanoic acid (AP5, 25 mM, Abcam) were diluted in sterile saline and 0.5 μL was injected to each side of the brain, whereas a similar volume of saline was injected intracranially in the control group. Rapamycin (10 nmol per 0.5 μL, Sigma-Aldrich) or saline was delivered into the PL-PFC approximately 30 min prior to intraperitoneal ketamine infusions.

Viral construction and packaging—Recombinant adeno-associated virus (AAV) vectors were serotyped with AAV1 coat proteins, packaged at Addgene viral vector manufacturing facilities. Viral titers were approximately 5×10^{12} particles per milliliter for pENN.AAV1.CamkII.GCaMP6f.WPRE.SV40, pENN.AAV1.CaMKIIa.eNpHR.3.0.EYFP., and pENN.AAV1.CamKII(1.3).eYFP.WPRE.hGH. Aliquots were stored light protected in a freezer before use.

Intracranial viral injections—As described in previous experiments (Lee et al., 2015), rats were anesthetized with 1.5%–2% isoflurane. Virus was delivered to the PL-PFC only. Rats were unilaterally or bilaterally injected with 0.65 μL viral vectors at a rate of 0.1 μL/20 s with a 26G 1 μL Hamilton syringe at anteroposterior (AP) +2.9 mm, mediolateral (ML) ± 1.6 mm, and dorsoventral (DV) −3.7 mm, with the tips angled 17° toward the midline

as described in previous experiments (Dale et al., 2018). After the virus was injected, the microinjection needles were left in place for 10 min before being raised 1 mm, therefore allowing for diffusion of virus particles and minimization of the spread of viral particles along the injection tract. The microneedle was left in place for an additional 5 min before being slowly raised out of the brain. Rats that were bilaterally injected with viral particle solution were next implanted bilaterally with 200 μm optic fibers held in 2.5 mm ferrules (Thorlabs) in the PL-PFC at AP +2.9 mm, ML ± 1.6 mm, and DV −3.2 mm, with the tips angled at 17° toward the midline. Fibers with ferrules were held in place by dental acrylic.

Gradient-index lens implantation and mounting—4–6 weeks after unilateral intracranial viral pENN.AAV1.CamkII.GCaMP6f.WPRE.SV40. injections, rats were anesthetized with 1.5%–2% isoflurane. Rats were stereotaxically implanted with the gradient-index (GRIN) lens (1.0 mm diameter, ~9.0 mm length, Inscopix) at AP +2.9 mm, ML ± 1.6 mm, and DV −3.5 mm, with the tips angled at 17° toward the midline, placing the lens ~100–300 μm above the imaging plane. The gap between the placement of the lens and the opening of the craniotomy site was filled with silicone elastomer (Kwik-Sil, World Precision Instruments). Lenses were held in place by dental acrylic.

Two weeks following the lens implantation, rats were anesthetized with 0.5%–1% isoflurane to be inspected for GCaMP6f fluorescence and Ca^{2+} transient activity. Rats were confirmed to be responsive while lightly anesthetized by retraction of paw after it has been pinched. The miniature microscope (nVoke, Inscopix) with a baseplate attached was stereotactically adjusted relative to the GRIN lens implantation to determine an optimal field of view (FOV) to image neural activity. Rats who exhibited neural responses to both auditory (clapping) and sensory (tail pinching) stimuli then proceeded to have a baseplate mounted. The anesthesia was raised to 1.5%–2% isoflurane. The baseplate was held in place with adhesive cement (Metabond Quick! Adhesive Cement System, C&B) and then a baseplate cover (Inscopix) was attached to the baseplate to protect the GRIN lens when not imaging.

GRIN lens imaging procedure—At the start of each imaging session, the rat is placed within the recording chamber over a mesh table, as described previously (Zhang et al., 2017) and the miniature microscope is mounted by aligning the FOV to the previous session FOV. Spontaneous neural activity is first recorded while the mouse habituated to, and freely moved within, the testing box without any experimenter-delivered stimuli. Noxious stimulation was applied by pricking the plantar surface of the hind paw contralateral to the brain recording site with pin prick by a 27-gauge needle (PP) in free-moving rats. Noxious stimulation was terminated by withdrawal of the paw. Non-noxious stimulation was applied to the same hind paw using a 0.4 g von Frey filament (vF) continuously for 1 s or until paw withdrawal. There were no withdrawal responses to von Frey in the majority of cases. All of the recording sessions consisted of approximately 7 trials of vF stimulation and then subsequently 7 trials of PP stimulation with variable inter-trial intervals of approximately 60 s to avoid sensitization. A video camera (HC-V550, Panasonic) was used to record the experiments. No behavioral sensitization or physical damage to the paws was observed.

Imaging experiments involving the CFA condition were performed 2 days after CFA injection. Imaging experiments involving the CFA + ketamine or saline condition were performed 4 days after CFA injection.

GRIN lens data acquisition—All miniature fluorescent microscope videos were recorded with a fluorescence power of 0.5–0.8 mW/mm^2 at a frame rate of 20 Hz at 1280 × 800. Following acquisition, raw videos were spatially downsampled by a binning factor of 4 (16x spatial downsample) and temporally downsampled by a binning factor of 2 (down to 10 frames per second) using Inscopix Data Processing Software (Inscopix). Furthermore, the videos were motion-corrected with reference to a single reference frame to match the XY positions of each frame throughout the video using Inscopix Data Processing Software in order to correct for motion artifacts. The motion-corrected 10 Hz video of raw Ca^{2+} activity was then saved as a .TIFF and used for cell identification. Ca^{2+} signals were extracted using modified constrained non-negative matrix factorization scripts in MATLAB (Pnevmatikakis et al., 2016; Zhou et al., 2018b), which allows for denoising, deconvolving, and demixing of microendoscopic imaging data in order to estimate temporally constrained instances of calcium activity for each neuron. Cross-session neurons were matched using CellReg through comparison of contours and centroid locations (Sheintuch et al., 2017).

Calcium response analyses—Trial-averaged Ca^{2+} fluorescence traces were obtained for individual neurons by z-scoring each trial from −5 to 5 s where 0 denotes time of peripheral stimulation (i.e., vF or PP). Each point in the trial was z-scored by subtracting the mean and dividing by the standard deviation of a baseline period of −5 to −3 s before peripheral stimulation. Z-scored trials were then added together and divided by the total number of trials to produce a single trial-averaged Ca^{2+} fluorescence trace for a neuron. For a given session, trial-averaged Ca^{2+} fluorescence traces from individual neurons were added together and divided by the total number of neurons to produce a single average trace of neuronal activity.

The peak Ca^{2+} fluorescence ΔF of a neuron was obtained by analyzing the post stimulus range from 0 to 5 s where 0 denotes time of peripheral stimulation. Each trial was z-scored by subtracting the mean and dividing by the standard deviation of a baseline range of −5 to −3 s before peripheral stimulation. The z-scored trial was then binned into 100 ms bins. A 2 s moving window was used to determine the maximum average Ca^{2+} fluorescence from the trial. The maximum average Ca^{2+} fluorescence was then averaged across all trials to produce a singular value for the peak post-stimulus activity of a neuron in a given session.

Immunohistochemistry—Rats were deeply anesthetized with isoflurane and transcardially perfused with ice-cold PBS and paraformaldehyde (PFA). After extraction, brains were fixed in PFA overnight and then cryoprotected in 30% sucrose in PBS for 48 h or until sinking (Lee et al., 2015). 20 μm coronal sections were washed in PBS and coverslipped with Fluoromount mounting medium (Sigma-Aldrich). Images containing cannula were stained with cresyl violet. Images were acquired with an Axio Zoom widefield microscope (Carl Zeiss).

Animal behavioral tests—Behavioral tests involving optogenetic stimulation were conducted approximately 4–5 weeks after viral injection of halorhodopsin (NpHR). Prior to each experiment, optic fibers were connected to a laser diode (Shanghai Dream Lasers Technology) through a mating sleeve, as described previously (Lee et al., 2015). Continuous laser light was delivered as a continuous laser using a transistory-transistor logic (TTL) pulse generator (Doric Lenses) with the laser output fiber tip fluorescence power of 6 mW. The measured power output for the laser was prior to insertion into the adaptor that connects to the intracranial optic fiber. Laser diodes of wavelength 589 nm were used for NpHR. The experimenters were blinded to the conditions of the treatment.

Conditioned place aversion assay—Conditioned Place Aversion (CPA) experiments were conducted similarly to those described previously (Zhang et al., 2017). A standard two-compartment apparatus was used consisting of two compartments of equal size. Different scents from balms were applied to the walls of the chambers to provide contextual cues. The two different compartments were connected with an opening large enough for a rat to travel through freely on top of a metal mesh table. The CPA protocol included preconditioning (baseline), conditioning, and testing phases. The preconditioning phase was 10 min, and animals spending > 480 s or < 120 s of the total time in either chamber during the preconditioning phase were eliminated from further analysis. Immediately following the preconditioning phase, the rats underwent conditioning. During conditioning (20 min), one of the two chambers was paired with peripheral stimulation (PP), or both chambers were paired with PP, or one chamber was paired with continuous optogenetic stimulation. The peripheral stimulus was repeated every 30 s. The order of peripheral stimulation and optogenetic activation was counterbalanced, e.g., half of the rats received optogenetic activation first, whereas the other half received control treatment first during conditioning. Likewise, chamber pairings were counterbalanced. During the testing phase, rats were allowed free access to both chambers again without any peripheral stimulations. Movements of the rats in each chamber were recorded by a camera and was analyzed with ANY-maze software. Decreased time spent in a chamber during the test phase as compared with the baseline indicated avoidance (aversion) of that chamber, whereas increased time spent in a chamber during the test phase as compared with the baseline indicated preference for that chamber.

Mechanical allodynia test—Mechanical allodynia was measured using a Dixon up-down method with vF filaments. Rats were placed individually into plexiglass chambers over a mesh table and allowed to acclimate for 20 mins prior to testing. vF filaments were applied to the paw of rats with logarithmically incremental stiffness, as described previously (Goffer et al., 2013). 50% withdrawal thresholds were calculated.

Cannula implantation and intracranial injections—For cannula implantations, rats were anesthetized with 1.5%–2% isoflurane. Rats were bilaterally implanted with two 26 gauge guide cannulas (P1 Technologies, Roanoke, VA) in the PL-PFC at AP +2.9 mm, ML ± 1.6 mm, and DV −2.2 mm, with the tips angled at 20° toward the midline. Cannulas were held in place by dental acrylic and were protected with occlusion stylets. For intracranial injections, solutions of either AP5, rapamycin, or saline were loaded into two 30 cm PE-50

tubes attached to a distilled water-filled 10 μL Hamilton's syringe. At the other end of the PE-50 tubes was a 33 gauge injector cannula that extended 1 mm past the implanted guides. The solutions were injected over 100 s and following the completion of injection, the implants were left in place for 60 s in order for proper diffusion of the solution in the brain. Prior to the beginning of the experiment, occlusion stylets were replaced.

QUANTIFICATION AND STATISTICAL ANALYSIS

Statistical tests—Results were given as mean ± SEM. To compare mechanical allodynia withdrawal thresholds for CFA-treated, ketamine-treated, and control rats, a two-way ANOVA with repeated-measures and post hoc multiple pairwise comparison Bonferroni tests or unpaired t tests were used whenever appropriate. For the CPA assay, a paired Student's t test was used to compare the time spent in each treatment chamber before and after conditioning (i.e., preconditioning versus test phase for each chamber). A two-tailed unpaired Student's t test was used to compare differences in CPA scores under various testing conditions. Sample sizes were determined so as to be comparable with previous studies.

When comparing groups of neurons, a paired Student's t test was used to compare paired data of neurons recorded in a single session, whereas an unpaired Student's t test was used to compare unpaired data of neurons recorded in separate sessions. To analyze the neuron population changes for pain response, a Fisher's exact test was used. Values of n and p are noted in the Figure Legends.

To define a neuron that altered its firing rate in response to a peripheral stimulus, the following method was used. Peripheral stimulations (i.e., vF or PP) were administered to the paw contralateral to CFA injections. For each trial, the raw time series was z-scored based on a baseline range of 4.5 to 1.5 s before stimulation. The z-scored time series from −5 to 5 s from the stimulus was binned into 100 ms bins. A 2 s window from 5 to 3 s before stimulus was used as the pre-stimulus value. The 2 s moving window from 0 to 5 s post-stimulus with the maximum value was used as the post-stimulus value. A one-tailed Wilcoxon rank sum test was then performed between pre- and post-stimulus values over all peripheral stimulations and the neuron was considered pain-responsive if $p < 0.025$.

Significance was defined at a level of a p value < 0.05 for all of the statistical tests used in the study. GraphPad Prism 8 (GraphPad Software) and MATLAB (MathWorks) were used to calculate statistical significance and GraphPad Prism 8 software was used to plot all of the graphs.

Cross-correlation statistics—Using CNMF_E software (https://github.com/zhoupc/CNMF_E) raw traces are extracted from Inscopix imaging data. The raw data are a scaled version of ΔF. Data consisted of three sessions for each rat from the naive, CFA, and CFA + ketamine condition respectively. To ensure consistency across all sessions for a given rat, the length of each time series was trimmed based on the session with the shortest recording time, lasting about 5 min (Figure 3A, Step 1). The times series was then normalized using the *normalize* function in MATLAB (Figure 3A, Step 2). A well-established and efficient spike deconvolution method (Friedrich et al., 2017; https://github.com/zhoupc/

OASIS_matlab) was used to obtain the proxy of spiking data from the normalized time series for each neuron (Figure 3A, Step 3).

The spiking data were then used as the input for the *xcorr* function in MATLAB to calculate a cross-correlation value between two time series (Figure 3A, Step 3). A lag of 10 was used and the maximum value was added to the undirected cross-correlation matrix. We used two independent statistical methods, a Monte Carlo simulation method and a bootstrap method, to determine if the cross-correlation value was statistically significant. For the Monte Carlo simulation method, one time series was randomly shuffled and a cross-correlation value was calculated between the shuffled time series and the second time series over 1000 iterations (Figure 3A, Step 4). The 1000 values were then ordered from the smallest to the largest and if the cross-correlation value from the original two time series was greater than the 950^{th} element the value was included in the matrix, producing a matrix populated with only statistically significant ($p < 0.05$) cross-correlation values (Figure 3A, Step 5). This cross-correlation matrix was then used to generate a graph to obtain network statistics, as explained in the next section (Figure 3A, Step 6).

To test the reliability of the Monte Carlo method we compared the results with the bootstrap method for determining statistically significant cross-correlation values. We calculated the 95% bootstrap confidence interval for the maximum cross-correlation value of the *xcorr* function in MATLAB with a lag of 10 over 1000 samples. We then used the 95% confidence interval as a threshold to determine if the cross-correlation value was statistically significant. We found that the network statistics were nearly identical between using the Monte Carlo method and using the bootstrap method. Therefore, we decided to use the Monte Carlo method in the remaining statistical analyses. In addition, to test the robustness of cross-correlation in the presence of data non-stationarity, we divided the time series in half and calculated the network statistics for each half independently. We found that both halves shared the same network statistics, suggesting that the cross-correlation statistics were stable over the recording session.

Subsampling analysis—Subsampling analysis is an effective statistical method for dealing with high-dimensional neural data. Since the number of recorded neurons varied between recording sessions and animals, we designed a neuronal subsampling procedure to account for the variability of sample sizes of pain-responsive and nonresponsive PL-PFC neurons. Depending on the total sample size of recording neurons in each session, we predetermined a ratio of pain-responsive to nonresponsive neurons. For each population group, we sorted the neurons based on their mean baseline firing rates and constructed two cumulative distribution functions (CDFs). In the CDF plot, the x axis shows the range of mean firing rates, and the y axis is the distribution percentile from 0 to 1. To accommodate neurons with diverse firing rates, we used an “inverse transform sampling” strategy to uniformly draw random variables from 0 and 1, and then mapped those values to the firing rate axis by an inverse CDF (Figure 3B). From each selected subsample, we computed graph-network statistics, and repeated the subsampling procedure 100 times. The complete subsampling analysis was conducted for both pain-responsive and nonresponsive groups, and repeated for all baseline, inflammatory pain, and ketamine conditions.

Graph-network statistics—In order to analyze the network statistics in each condition we used Gephi (https://gephi.org/), an open-source network and graph analysis software that allows for 3D graph visualization. Graph visualizations consist of nodes, representatives of the neurons in the network, and edges, connections between neurons with significant cross-correlations. We focused specifically on degree centrality, C_D, the number of edges connected to a node, and betweenness centrality, C_B, a measure of the volume of shortest paths that pass though the given node (De Vico Fallani et al., 2014; Kwon et al., 2019). These two network statistics allow us to identify neurons that act as hubs for information flow in a network, as shown in prior studies (Bilbao et al., 2018; Komaki et al., 2016; Minati et al., 2013; Redcay et al., 2013). For our study specifically, C_B and $C_{D,}$ provide insight into how the role of pain responsive neurons in a network change on a population level in the presence of inflammatory pain and after a sub-anesthetic dose of ketamine.

To analyze the connections between neurons across all three conditions, we subsampled a set percentage of pain and nonresponsive neurons for a given rat. The number of subsampled pain and nonresponsive neurons was jointly determined based on the number of pain responsive neurons and total number of neurons across all sessions for a given rat. In order to subsample neurons from each group, pain responsive or nonresponsive, we ordered the neurons by their average firing rates and then uniformly selected a subsample of PL-PFC neurons to ensure a mixture of high and low firing neurons (Figure 3B). The uniform subsampling procedure was designed to account for the variability in the number of recorded neurons and the percentage of pain-responsive neurons between recording sessions. After N subsampled neurons were selected, we computed the corresponding cross-correlation matrix of NxN, and all values greater than or equal to 0.1 were kept for visualization. The matrix was then converted into a .gdf file containing information about N nodes and $N(N\text{-}1)$ edges to be displayed in the network as an input for Gephi. The pain-responsive neurons were always added as the first set of nodes in the graph so they could be easily identified.

After subsampling for a certain percentage of pain responsive neurons and nonresponsive neurons, we calculated the median network statistic for C_B and C_D of the nodes corresponding to the pain responsive neurons and nonresponsive neurons, respectively. For each of the three conditions, we repeated this sampling process 100 times and calculated the mean of the 100 subsampling's to obtain a single value from each condition. To obtain normalized C_D for rat 1, the median degree from each subsampling was divided by n-1, where n denotes the total number of subsampled neurons, for pain and nonresponsive neurons, independently. To obtain relative C_B and relative C_D, the naive condition was set to 1 and the average statistics from the other conditions were rescaled with respect to the naive condition. For all of the methods above, significant changes in network statistics between the naive, CFA and CFA + ketamine conditions were evaluated using an ordinary one-way ANOVA with Bonferroni's multiple comparisons test. To test for significance between CFA and CFA + ketamine or CFA + saline, unpaired t tests were used.

Supplementary Material

Refer to Web version on PubMed Central for supplementary material.

ACKNOWLEDGMENTS

The work was supported by NIH (GM115384 to J.W.).

REFERENCES

Acuña MA, Kasanetz F, De Luna P, and Nevian T (2020). Cortical representation of pain by stable dedicated neurons and dynamic ensembles. bio-Rxiv. 10.1101/2020.11.02.364778.

Alonso R, Brocas I, and Carrillo JD (2014). Resource Allocation in the Brain. Rev. Econ. Stud 81, 501–534.

Apkarian AV, Sosa Y, Sonty S, Levy RM, Harden RN, Parrish TB, and Gitelman DR (2004). Chronic back pain is associated with decreased prefrontal and thalamic gray matter density. J. Neurosci 24, 10410–10415. [PubMed: 15548656]

Autry AE, Adachi M, Nosyreva E, Na ES, Los MF, Cheng PF, Kavalali ET, and Monteggia LM (2011). NMDA receptor blockade at rest triggers rapid behavioural antidepressant responses. Nature 475, 91–95. [PubMed: 21677641]

Baliki MN, Petre B, Torbey S, Herrmann KM, Huang L, Schnitzer TJ, Fields HL, and Apkarian AV (2012). Corticostriatal functional connectivity predicts transition to chronic back pain. Nat. Neurosci 15, 1117–1119. [PubMed: 22751038]

Basbaum AI, Bautista DM, Scherrer G, and Julius D (2009). Cellular and molecular mechanisms of pain. Cell 139, 267–284. [PubMed: 19837031]

Bays PM, and Husain M (2008). Dynamic shifts of limited working memory resources in human vision. Science 321, 851–854. [PubMed: 18687968]

Berman RM, Cappiello A, Anand A, Oren DA, Heninger GR, Charney DS, and Krystal JH (2000). Antidepressant effects of ketamine in depressed patients. Biol. Psychiatry 47, 351–354. [PubMed: 10686270]

Bilbao A, Falfán-Melgoza C, Leixner S, Becker R, Singaravelu SK, Sack M, Sartorius A, Spanagel R, and Weber-Fahr W (2018). Longitudinal Structural and Functional Brain Network Alterations in a Mouse Model of Neuropathic Pain. Neuroscience 387, 104–115. [PubMed: 29694917]

Bonifazi P, and Massobrio P (2019). Reconstruction of Functional Connectivity from Multielectrode Recordings and Calcium Imaging. Adv. Neurobiol 22, 207–231. [PubMed: 31073938]

Bruning AL, and Lewis-Peacock JA (2020). Long-term memory guides resource allocation in working memory. Sci. Rep 10, 22161. [PubMed: 33335170]

Chen LM, Friedman RM, and Roe AW (2009). Area-specific representation of mechanical nociceptive stimuli within SI cortex of squirrel monkeys. Pain 141, 258–268. [PubMed: 19136211]

Cheriyan J, and Sheets PL (2018). Altered Excitability and Local Connectivity of mPFC-PAG Neurons in a Mouse Model of Neuropathic Pain. J. Neurosci 38, 4829–4839. [PubMed: 29695413]

Chudler EH, Anton F, Dubner R, and Kenshalo DR Jr. (1990). Responses of nociceptive SI neurons in monkeys and pain sensation in humans elicited by noxious thermal stimulation: effect of interstimulus interval. J. Neurophysiol 63, 559–569. [PubMed: 2329361]

Cohen SP, Bhatia A, Buvanendran A, Schwenk ES, Wasan AD, Hurley RW, Viscusi ER, Narouze S, Davis FN, Ritchie EC, et al. (2018). Consensus Guidelines on the Use of Intravenous Ketamine Infusions for Chronic Pain From the American Society of Regional Anesthesia and Pain Medicine, the American Academy of Pain Medicine, and the American Society of Anesthesiologists. Reg. Anesth. Pain Med 43, 521–546. [PubMed: 29870458]

Corder G, Ahanonu B, Grewe BF, Wang D, Schnitzer MJ, and Scherrer G (2019). An amygdalar neural ensemble that encodes the unpleasantness of pain. Science 363, 276–281. [PubMed: 30655440]

Craig AD, Bushnell MC, Zhang ET, and Blomqvist A (1994). A thalamic nucleus specific for pain and temperature sensation. Nature 372, 770–773. [PubMed: 7695716]

Cramer JV, Gesierich B, Roth S, Dichgans M, Düring M, and Liesz A (2019). In vivo widefield calcium imaging of the mouse cortex for analysis of network connectivity in health and brain disease. Neuroimage 199, 570–584. [PubMed: 31181333]

Dale J, Zhou H, Zhang Q, Martinez E, Hu S, Liu K, Urien L, Chen Z, and Wang J (2018). Scaling Up Cortical Control Inhibits Pain. Cell Rep. 23, 1301–1313. [PubMed: 29719246]

De Vico Fallani F, Richiardi J, Chavez M, and Achard S (2014). Graph analysis of functional brain networks: practical issues in translational neuroscience. Philos. Trans. R. Soc. Lond. B Biol. Sci 369, 20130521. [PubMed: 25180301]

Doan LV, and Wang J (2018). An Update on the Basic and Clinical Science of Ketamine Analgesia. Clin. J. Pain 34, 1077–1088. [PubMed: 29927768]

Friedrich J, Zhou P, and Paninski L (2017). Fast online deconvolution of calcium imaging data. PLoS Comput. Biol 13, e1005423. [PubMed: 28291787]

Fusi S, Miller EK, and Rigotti M (2016). Why neurons mix: high dimensionality for higher cognition. Curr. Opin. Neurobiol 37, 66–74. [PubMed: 26851755]

Garcia LS, Comim CM, Valvassori SS, Réus GZ, Barbosa LM, Andreazza AC, Stertz L, Fries GR, Gavioli EC, Kapczinski F, and Quevedo J (2008). Acute administration of ketamine induces antidepressant-like effects in the forced swimming test and increases BDNF levels in the rat hippocampus. Prog. Neuropsychopharmacol. Biol. Psychiatry 32, 140–144. [PubMed: 17884272]

Geha PY, Baliki MN, Harden RN, Bauer WR, Parrish TB, and Apkarian AV (2008). The brain in chronic CRPS pain: abnormal gray-white matter interactions in emotional and autonomic regions. Neuron 60, 570–581. [PubMed: 19038215]

Goffer Y, Xu D, Eberle SE, D'amour J, Lee M, Tukey D, Froemke RC, Ziff EB, and Wang J (2013). Calcium-permeable AMPA receptors in the nucleus accumbens regulate depression-like behaviors in the chronic neuropathic pain state. J. Neurosci 33, 19034–19044. [PubMed: 24285907]

Huang J, Gadotti VM, Chen L, Souza IA, Huang S, Wang D, Ramakrishnan C, Deisseroth K, Zhang Z, and Zamponi GW (2019). A neuronal circuit for activating descending modulation of neuropathic pain. Nat. Neurosci 22, 1659–1668. [PubMed: 31501573]

Ji G, and Neugebauer V (2011). Pain-related deactivation of medial prefrontal cortical neurons involves mGluR1 and GABA(A) receptors. J. Neurophysiol 106, 2642–2652. [PubMed: 21880942]

Johansen JP, and Fields HL (2004). Glutamatergic activation of anterior cingulate cortex produces an aversive teaching signal. Nat. Neurosci 7, 398–403. [PubMed: 15004562]

Johansen JP, Fields HL, and Manning BH (2001). The affective component of pain in rodents: direct evidence for a contribution of the anterior cingulate cortex. Proc. Natl. Acad. Sci. USA 98, 8077–8082. [PubMed: 11416168]

Kano M, Grinsvall C, Ran Q, Dupont P, Morishita J, Muratsubaki T, Mugikura S, Ly HG, Törnblom H, Ljungberg M, et al. (2020). Resting state functional connectivity of the pain matrix and default mode network in irritable bowel syndrome: a graph theoretical analysis. Sci. Rep 10, 11015. [PubMed: 32620938]

Kelly CJ, Huang M, Meltzer H, and Martina M (2016). Reduced Glutamatergic Currents and Dendritic Branching of Layer 5 Pyramidal Cells Contribute to Medial Prefrontal Cortex Deactivation in a Rat Model of Neuropathic Pain. Front. Cell. Neurosci 10, 133. [PubMed: 27252623]

Kenshalo DR, Iwata K, Sholas M, and Thomas DA (2000). Response properties and organization of nociceptive neurons in area 1 of monkey primary somatosensory cortex. J. Neurophysiol 84, 719–729. [PubMed: 10938299]

King T, Vera-Portocarrero L, Gutierrez T, Vanderah TW, Dussor G, Lai J, Fields HL, and Porreca F (2009). Unmasking the tonic-aversive state in neuropathic pain. Nat. Neurosci 12, 1364–1366. [PubMed: 19783992]

Kobak D, Brendel W, Constantinidis C, Feierstein CE, Kepecs A, Mainen ZF, Qi XL, Romo R, Uchida N, and Machens CK (2016). Demixed principal component analysis of neural population data. eLife 5, e10989. [PubMed: 27067378]

Komaki Y, Hikishima K, Shibata S, Konomi T, Seki F, Yamada M, Miyasaka N, Fujiyoshi K, Okano HJ, Nakamura M, and Okano H (2016). Functional brain mapping using specific sensory-circuit stimulation and a theoretical graph network analysis in mice with neuropathic allodynia. Sci. Rep 6, 37802. [PubMed: 27898057]

Kwon H, Choi YH, and Lee JM (2019). A Physarum Centrality Measure of the Human Brain Network. Sci. Rep 9, 5907. [PubMed: 30976010]

Lee M, Manders TR, Eberle SE, Su C, D'amour J, Yang R, Lin HY, Deisseroth K, Froemke RC, and Wang J (2015). Activation of corticostriatal circuitry relieves chronic neuropathic pain. J. Neurosci 35, 5247–5259. [PubMed: 25834050]

Li N, Lee B, Liu RJ, Banasr M, Dwyer JM, Iwata M, Li XY, Aghajanian G, and Duman RS (2010). mTOR-dependent synapse formation underlies the rapid antidepressant effects of NMDA antagonists. Science 329, 959–964. [PubMed: 20724638]

Machado-Vieira R, Salvadore G, Diazgranados N, and Zarate CA Jr. (2009). Ketamine and the next generation of antidepressants with a rapid onset of action. Pharmacol. Ther 123, 143–150. [PubMed: 19397926]

Maeng S, Zarate CA Jr., Du J, Schloesser RJ, McCammon J, Chen G, and Manji HK (2008). Cellular mechanisms underlying the antidepressant effects of ketamine: role of alpha-amino-3-hydroxy-5-methylisoxazole-4-propionic acid receptors. Biol. Psychiatry 63, 349–352. [PubMed: 17643398]

Markowitz DA, Curtis CE, and Pesaran B (2015). Multiple component networks support working memory in prefrontal cortex. Proc. Natl. Acad. Sci. USA 112, 11084–11089. [PubMed: 26283366]

Martinez E, Lin HH, Zhou H, Dale J, Liu K, and Wang J (2017). Corticostriatal Regulation of Acute Pain. Front. Cell. Neurosci 11, 146. [PubMed: 28603489]

Minati L, Varotto G, D'Incerti L, Panzica F, and Chan D (2013). From brain topography to brain topology: relevance of graph theory to functional neuroscience. Neuroreport 24, 536–543. [PubMed: 23660679]

Moayedi M, Weissman-Fogel I, Crawley AP, Goldberg MB, Freeman BV, Tenenbaum HC, and Davis KD (2011). Contribution of chronic pain and neuroticism to abnormal forebrain gray matter in patients with temporomandibular disorder. Neuroimage 55, 277–286. [PubMed: 21156210]

Murray JD, Bernacchia A, Roy NA, Constantinidis C, Romo R, and Wang XJ (2017). Stable population coding for working memory coexists with heterogeneous neural dynamics in prefrontal cortex. Proc. Natl. Acad. Sci. USA 114, 394–399. [PubMed: 28028221]

Mutso AA, Radzicki D, Baliki MN, Huang L, Banisadr G, Centeno MV, Radulovic J, Martina M, Miller RJ, and Apkarian AV (2012). Abnormalities in hippocampal functioning with persistent pain. J. Neurosci 32, 5747–5756. [PubMed: 22539837]

Navratilova E, Xie JY, Meske D, Qu C, Morimura K, Okun A, Arakawa N, Ossipov M, Fields HL, and Porreca F (2015). Endogenous opioid activity in the anterior cingulate cortex is required for relief of pain. J. Neurosci 35, 7264–7271. [PubMed: 25948274]

Petzke F, Clauw DJ, Ambrose K, Khine A, and Gracely RH (2003). Increased pain sensitivity in fibromyalgia: effects of stimulus type and mode of presentation. Pain 105, 403–413. [PubMed: 14527701]

Ploner M, Schmitz F, Freund HJ, and Schnitzler A (2000). Differential organization of touch and pain in human primary somatosensory cortex. J. Neurophysiol 83, 1770–1776. [PubMed: 10712498]

Pnevmatikakis EA, Soudry D, Gao Y, Machado TA, Merel J, Pfau D, Reardon T, Mu Y, Lacefield C, Yang W, et al. (2016). Simultaneous denoising, deconvolution, and demixing of calcium imaging data. Neuron 89, 285–299. [PubMed: 26774160]

Radzicki D, Pollema-Mays SL, Sanz-Clemente A, and Martina M (2017). Loss of M1 Receptor Dependent Cholinergic Excitation Contributes to mPFC Deactivation in Neuropathic Pain. J. Neurosci 37, 2292–2304. [PubMed: 28137966]

Rainville P, Duncan GH, Price DD, Carrier B, and Bushnell MC (1997). Pain affect encoded in human anterior cingulate but not somatosensory cortex. Science 277, 968–971. [PubMed: 9252330]

Ramirez-Cardenas A, and Viswanathan P (2016). The Role of Prefrontal Mixed Selectivity in Cognitive Control. J. Neurosci 36, 9013–9015. [PubMed: 27581444]

Redcay E, Moran JM, Mavros PL, Tager-Flusberg H, Gabrieli JD, and Whitfield-Gabrieli S (2013). Intrinsic functional network organization in high-functioning adolescents with autism spectrum disorder. Front. Hum. Neurosci 7, 573. [PubMed: 24062673]

Ren W, Centeno MV, Wei X, Wickersham I, Martina M, Apkarian AV, and Surmeier DJ (2021). Adaptive alterations in the mesoaccumbal network following peripheral nerve injury. Pain 162, 895–906. [PubMed: 33021562]

Rigotti M, Barak O, Warden MR, Wang XJ, Daw ND, Miller EK, and Fusi S (2013). The importance of mixed selectivity in complex cognitive tasks. Nature 497, 585–590. [PubMed: 23685452]

Salzman CD, and Fusi S (2010). Emotion, cognition, and mental state representation in amygdala and prefrontal cortex. Annu. Rev. Neurosci 33, 173–202. [PubMed: 20331363]

Scudds RA, Rollman GB, Harth M, and McCain GA (1987). Pain perception and personality measures as discriminators in the classification of fibrositis. J. Rheumatol 14, 563–569. [PubMed: 3476752]

Sheintuch L, Rubin A, Brande-Eilat N, Geva N, Sadeh N, Pinchasof O, and Ziv Y (2017). Tracking the Same Neurons across Multiple Days in Ca^{2+} Imaging Data. Cell Rep 21, 1102–1115. [PubMed: 29069591]

Singh A, Patel D, Li A, Hu L, Zhang Q, Liu Y, Guo X, Robinson E, Martinez E, Doan L, et al. (2020). Mapping Cortical Integration of Sensory and Affective Pain Pathways. Curr. Biol 30, 1703–1715.e5. [PubMed: 32220320]

Spisak T, Kincses B, Schlitt F, Zunhammer M, Schmidt-Wilcke T, Kincses ZT, and Bingel U (2020). Pain-free resting-state functional brain connectivity predicts individual pain sensitivity. Nat. Commun 11, 187. [PubMed: 31924769]

Sporns O (2018). Graph theory methods: applications in brain networks. Dialogues Clin. Neurosci 20, 111–121. [PubMed: 30250388]

Talay RS, Liu Y, Michael M, Li A, Friesner ID, Zeng F, Sun G, Chen ZS, Zhang Q, and Wang J (2021). Pharmacological restoration of anti-nociceptive functions in the prefrontal cortex relieves chronic pain. Prog. Neurobiol 201, 102001. [PubMed: 33545233]

Tommerdahl M, Delemos KA, Vierck CJ Jr., Favorov OV, and Whitsel BL (1996). Anterior parietal cortical response to tactile and skin-heating stimuli applied to the same skin site. J. Neurophysiol 75, 2662–2670. [PubMed: 8793772]

Vachon-Presseau E, Berger SE, Abdullah TB, Griffith JW, Schnitzer TJ, and Apkarian AV (2019). Identification of traits and functional connectivity-based neurotraits of chronic pain. PLoS Biol. 17, e3000349. [PubMed: 31430270]

Wang J, Goffer Y, Xu D, Tukey DS, Shamir DB, Eberle SE, Zou AH, Blanck TJ, and Ziff EB (2011). A single subanesthetic dose of ketamine relieves depression-like behaviors induced by neuropathic pain in rats. Anesthesiology 115, 812–821. [PubMed: 21934410]

Whitsel BL, Favorov OV, Li Y, Quibrera M, and Tommerdahl M (2009). Area 3a neuron response to skin nociceptor afferent drive. Cereb. Cortex 19, 349–366. [PubMed: 18534992]

Whitsel BL, Vierck CJ, Waters RS, Tommerdahl M, and Favorov OV (2019). Contributions of Nociresponsive Area 3a to Normal and Abnormal Somatosensory Perception. J. Pain 20, 405–419. [PubMed: 30227224]

Yang C, Hu YM, Zhou ZQ, Zhang GF, and Yang JJ (2013). Acute administration of ketamine in rats increases hippocampal BDNF and mTOR levels during forced swimming test. Ups. J. Med. Sci 118, 3–8. [PubMed: 22970723]

Yoo AH, Klyszejko Z, Curtis CE, and Ma WJ (2018). Strategic allocation of working memory resource. Sci. Rep 8, 16162. [PubMed: 30385803]

Zarate CA Jr., Singh JB, Carlson PJ, Brutsche NE, Ameli R, Lucken-baugh DA, Charney DS, and Manji HK (2006). A randomized trial of an N-methyl-D-aspartate antagonist in treatment-resistant major depression. Arch. Gen. Psychiatry 63, 856–864. [PubMed: 16894061]

Zhang Z, Gadotti VM, Chen L, Souza IA, Stemkowski PL, and Zamponi GW (2015). Role of Prelimbic GABAergic Circuits in Sensory and Emotional Aspects of Neuropathic Pain. Cell Rep. 12, 752–759. [PubMed: 26212331]

Zhang Q, Manders T, Tong AP, Yang R, Garg A, Martinez E, Zhou H, Dale J, Goyal A, Urien L, et al. (2017). Chronic pain induces generalized enhancement of aversion. eLife 6, e25302. [PubMed: 28524819]

Zhou W, Wang N, Yang C, Li XM, Zhou ZQ, and Yang JJ (2014). Ketamine-induced antidepressant effects are associated with AMPA receptors-mediated upregulation of mTOR and BDNF in rat hippocampus and prefrontal cortex. Eur. Psychiatry 29, 419–423. [PubMed: 24321772]

Zhou H, Zhang Q, Martinez E, Dale J, Hu S, Zhang E, Liu K, Huang D, Yang G, Chen Z, and Wang J (2018a). Ketamine reduces aversion in rodent pain models by suppressing hyperactivity of the anterior cingulate cortex. Nat. Commun 9, 3751. [PubMed: 30218052]

Zhou P, Resendez SL, Rodriguez-Romaguera J, Jimenez JC, Neufeld SQ, Giovannucci A, Friedrich J, Pnevmatikakis EA, Stuber GD, Hen R, et al. (2018b). Efficient and accurate extraction of in vivo calcium signals from microendoscopic video data. eLife 7, e28728. [PubMed: 29469809]

Highlights

- Inflammatory pain disrupts functional connectivity in the prefrontal cortex (PFC)
- Inflammatory pain reduces the overall nociceptive response of PFC neurons
- Ketamine restores functional connectivity and the nociceptive response of PFC neurons
- Ketamine produces anti-aversive effects by enhancing neural activities in the PFC

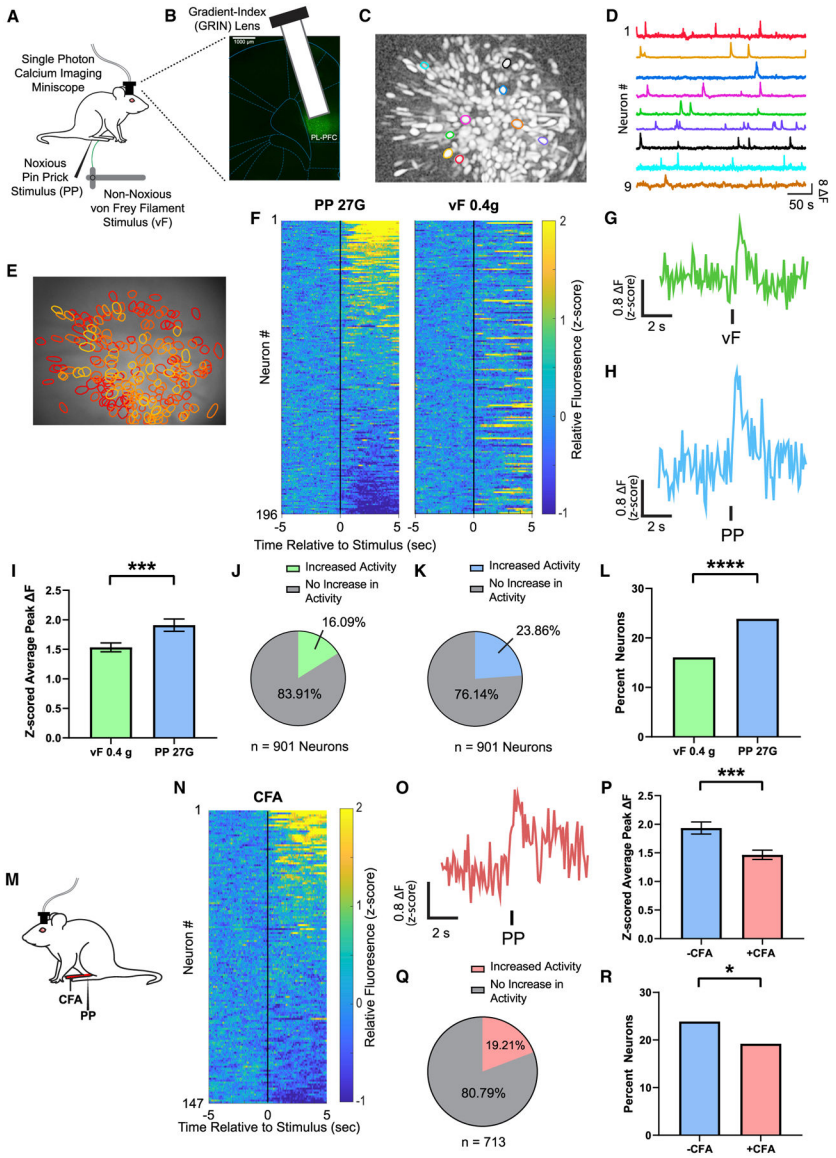

Figure 1. Inflammatory pain suppresses the PL-PFC response to acute noxious stimuli

(A) Schematic of calcium imaging experiments.

(B) Gradient-index (GRIN) lens placement and GCaMP6f expression. Scale bar, 1000 μm.

(C and D) Map of example identified contours in maximum projection image after motion correction and neural enhancement (C) with corresponding activity traces (D).

(E) Map of active PL-PFC neurons with overlaid contours over imaging field of view.

(F) Mean Ca^{2+} response (Z scored relative fluorescence) across all trials for all PL-PFC neurons imaged during a single session (n = 196 neurons) from the same rat. Neurons are aligned from high to low Ca^{2+} responses after acute noxious (PP) stimulus. Individual neuron identifications between PP and acute non-noxious (vF) stimulation are consistent across trial rows.

(G) Representative trace of analysis-derived activity of a single neuron during vF during a single session. See STAR Methods.

(H) Representative trace of analysis-derived activity of a single neuron during PP during a single session. See STAR Methods.
(I) Neurons in the PL-PFC show increased activity after administration of an acute pain stimulus. n = 901 neurons (9 rats); p = 0.0002, paired Student's t test. See STAR Methods.
(J) A total of 16.09% neurons in the PL-PFC, n = 901 neurons in 9 rats, showed a change in activity in response to vF. See STAR Methods.
(K) A total of 23.86% neurons in the PL-PFC, n = 901 neurons in 9 rats, showed a change in activity in response to PP. See STAR Methods.
(L) More PL-PFC neurons responded to PP than vF. $p < 0.0001$, Fisher's exact test. See STAR Methods.
(M) Schematic of the CFA model. Peripheral stimulation occurred on the paw contralateral to CFA injection.
(N) Mean Ca^{2+} response (Z scored relative fluorescence) across all trials for all PL-PFC neurons imaged during a single session (n = 147 neurons) from the same CFA-treated rat. Neurons are aligned from high to low Ca^{2+} responses after PP.
(O) A representative trace of analysis-derived activity of a single neuron during PP during a single session of a CFA-treated rat.
(P) After CFA administration, neurons in the PL-PFC showed a decrease in peak Ca^{2+} fluorescence in response to noxious stimulations. −CFA, n = 901 neurons (9 rats); +CFA, n = 713 neurons (9 rats); p = 0.0004, unpaired Student's t test.
(Q) A total of 19.21% neurons in the PL-PFC, n = 713 neurons in 9 rats, had a change in activity in response to PP after CFA.
(R) Inflammatory pain decreased the number of neurons in the PL-PFC that responded to noxious stimuli. p = 0.0249, Fisher's exact test.
Data represented as mean ± SEM.

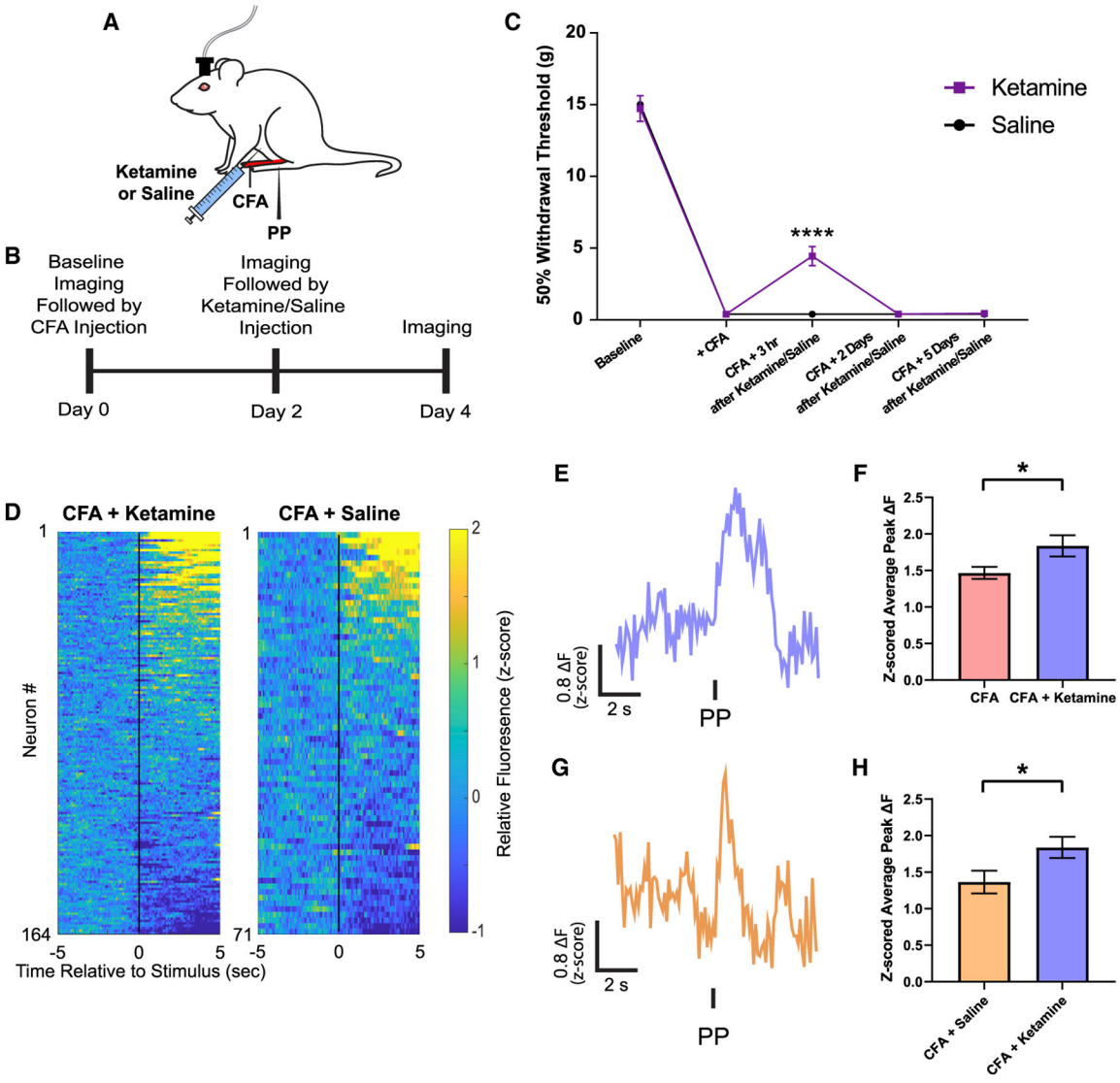

Figure 2. Ketamine restores the population nociceptive response in the PL-PFC in the inflammatory pain condition

(A) Schematic of ketamine pharmacology experiments in the CFA model.

(B) Time course for the endoscopic Ca^{2+} imaging in ketamine- or saline-treated rats.

(C) A single sub-anesthetic dose of ketamine (10 mg/kg) provided only transient relief of allodynia. n = 12; $p < 0.0001$, two-way ANOVA with repeated-measures and post hoc Bonferroni test.

(D) Left: mean Ca^{2+} response (*Z* scored relative fluorescence) across all trials for all PL-PFC neurons imaged during a single session (n = 164 neurons) from the same ketamine-treated rat. Neurons are aligned from high to low Ca^{2+} responses after PP. Right: mean Ca^{2+} response (*Z* scored relative fluorescence) across all trials for all PL-PFC neurons imaged during a single session (n = 71 neurons) from a saline-treated rat. Neurons are aligned from high to low Ca^{2+} responses after PP.

(E) A representative trace of analysis-derived activity of a single neuron during PP during a single session from a ketamine-treated rat.

(F) Ketamine treatment increased mean peak Ca^{2+} fluorescence in PL-PFC neurons compared to CFA rats without ketamine treatment. CFA, n = 713 neurons (9 rats); CFA + ketamine, n = 497 neurons (5 rats); p = 0.0176, unpaired Student's t test.
(G) A representative trace of analysis-derived activity of a single neuron during PP during a single session from a saline-treated rat.
(H) Ketamine treatment increased mean peak Ca^{2+} fluorescence in PL-PFC neurons compared to saline treatment. CFA + ketamine, n = 497 neurons (5 rats); CFA + saline, n = 222 neurons (4 rats); p = 0.0487, unpaired Student's t test.
Data represented as mean ± SEM.

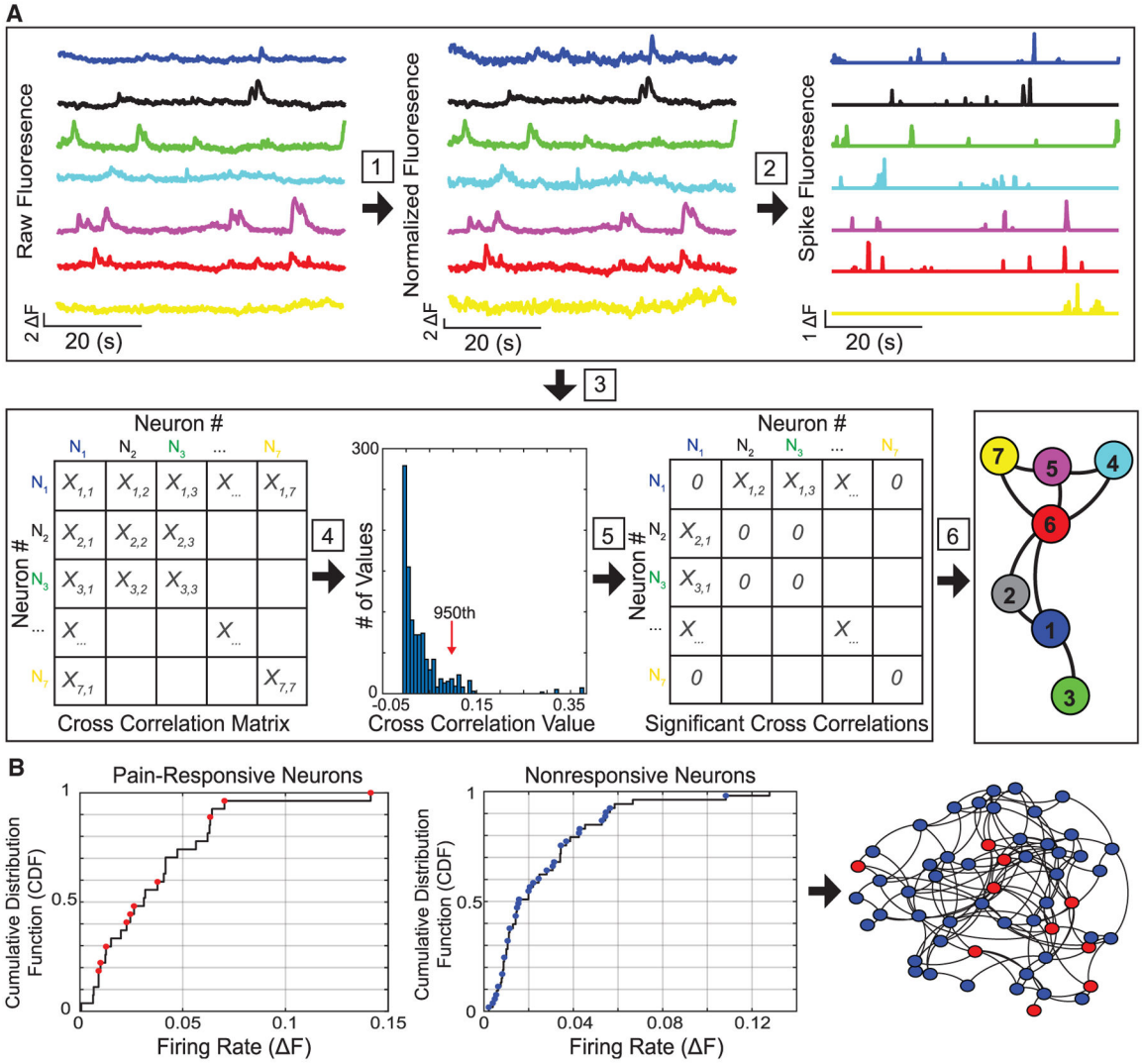

Figure 3. Application of functional connectivity analysis to subsampled PL-PFC neurons

(A) After ΔF Ca^{2+} fluorescence traces of imaged PL-PFC neurons from freely behaving rats were preprocessed, we conducted six analytic steps. A schematic of 7 PFC neurons is shown here. Step 1: Each raw trace was normalized. Step 2: A non-negative spike deconvolution method was used to extract the putative spiking activity of each neuron. Step 3: Nonzero-lag cross-correlation computation was conducted among neurons. Step 4: We determined statistically significant correlation coefficients using the Monte Carlo and bootstrap methods (see STAR Methods). Vertical line denotes the 95% significance threshold (i.e., Monte Carlo $p < 0.05$). Step 5: Non-significant correlation values were set to zeros. Step 6: We performed undirected neuronal graph visualization (Gephi) and computation of graph-theoretic network statistics.

(B) Neurons were classified based on pain responsiveness and further ordered based on their mean firing rates. Left: cumulative distribution function (CDF) was computed separately for pain-responsive and nonresponsive neurons, based on the average basal firing rates of respective populations. Next, for the purpose of subsampling pain-responsive or nonresponsive populations, we uniformly sampled neurons (red dots, pain-responsive

neurons; blue dots, nonresponsive neurons) from the CDF (i.e., inverse transform sampling, see STAR Methods) for further analysis, ensuring the inclusion of equitable distribution of firing rates among the chosen neurons. The subsampling procedure was designed to account for the variability of number of recorded neurons and the percentage of pain-responsive neurons between recording sessions. Right: the selected subsampled pain-responsive (red) and non-responsive (blue) neurons were formed into a schematic PFC subnetwork, where the connectivity of neuronal graph was determined by the significant cross-correlation coefficients.

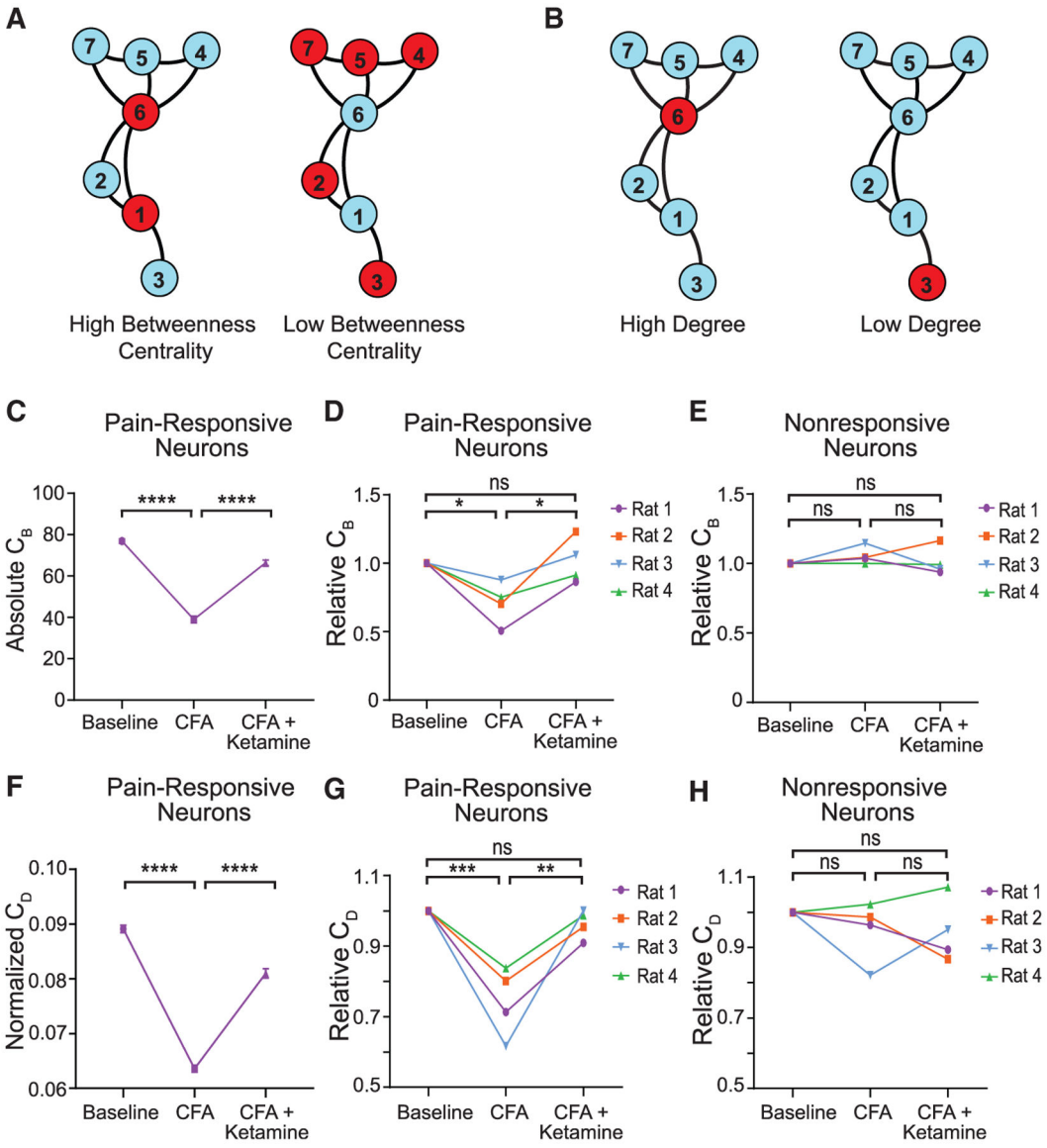

Figure 4. Ketamine restores betweenness centrality and degree centrality of pain-responsive neurons in the inflammatory pain condition

(A) Illustration of high versus low betweenness centrality (C_B). Left: nodes 6 and 1 have high betweenness centrality. Right: nodes 2, 3, 4, 5, and 7 have low betweenness centrality.

(B) Illustration of high versus low degree centrality (C_D). Left: node 6 has a high degree because it connects to five out of the six other neurons. Right: node 3 has a low degree because it only connects to one out of the six other neurons. Betweenness centrality (C_B) is calculated as the fraction of the number of the shortest paths passing through a given node or edge to the total number of shortest paths. The degree centrality (C_D) is defined as the number of edges connected to a node, and it is a measure to quantify the local centrality of each node (Kwon et al., 2019).

(C) Absolute C_B of pain-responsive neurons for rat 1 declined after CFA treatment, but recovered after ketamine treatment. n = 100 Monte Carlo runs of subsampling; $p < 0.0001$, one-way ANOVA with post hoc Bonferroni test.

(D) Relative C_B of pain-responsive neurons for all rats declined after CFA treatment, n = 4 rats; p = 0.0359, one-way ANOVA with post hoc Bonferroni test, but recovered after ketamine treatment. n = 4 rats; p = 0.0268, one-way ANOVA with post hoc Bonferroni test. Relative C_B was normalized with respect to the baseline condition, for pain-responsive neurons across all ketamine-treated rats.
(E) Relative C_B of pain nonresponsive neurons did not change after CFA treatment, n = 4 rats; p = 0.8354, one-way ANOVA with post hoc Bonferroni test, nor did it respond to ketamine treatment. n = 4 rats; p > 0.9999, one-way ANOVA with post hoc Bonferroni test.
(F) Normalized C_D of pain-responsive neurons for rat 1 declined after CFA treatment, but recovered after ketamine treatment. n = 100 Monte Carlo runs of subsampling; p < 0.0001, one-way ANOVA with post hoc Bonferroni test.
(G) Relative C_D of pain-responsive neurons for all rats declined after CFA treatment, n = 4 rats; p = 0.0007, one-way ANOVA with post hoc Bonferroni test, but recovered after ketamine treatment. n = 4 rats; p = 0.0020, one-way ANOVA with post hoc Bonferroni test. Relative C_B was normalized with respect to the baseline condition, for pain-responsive neurons across all ketamine-treated rats.
(H) Relative C_B of pain nonresponsive neurons did not change after CFA treatment, n = 4 rats; p > 0.9999, one-way ANOVA with post hoc Bonferroni test, nor did it respond to ketamine treatment. n = 4 rats; p > 0.9999, one-way ANOVA.
Data represented as mean ± SEM.

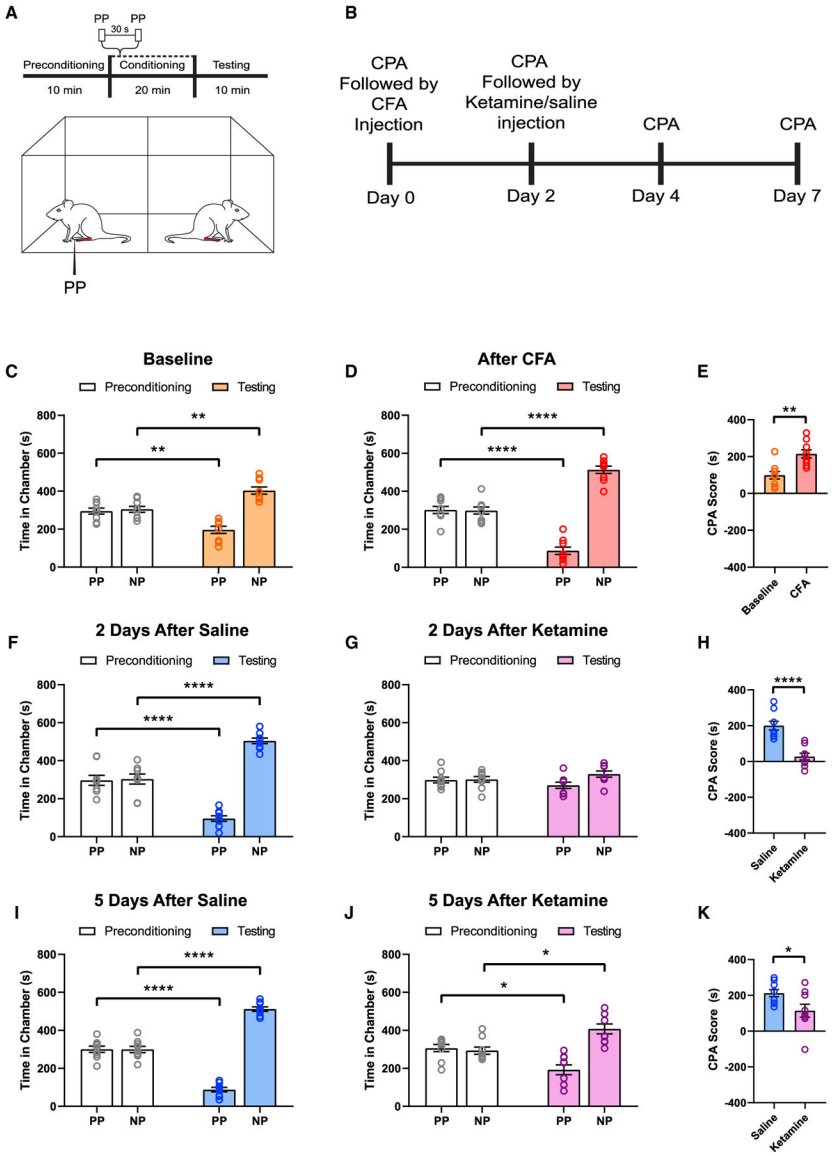

Figure 5. Ketamine inhibits aversive symptoms of inflammatory pain

(A) Schematic of conditioned place aversion (CPA) assay. During the conditioning phase, one of the chambers was paired with the acute noxious stimulus (PP), whereas the opposite chamber was not paired with a noxious stimulus (NP).

(B) Time course for CPA tests in ketamine- or saline-treated rats.

(C) At baseline, rats displayed avoidance of the chamber paired with the acute noxious stimulus (PP). n = 9; p = 0.0012, paired Student's t test.

(D) Rats treated with CFA displayed an increased avoidance of the chamber paired with the noxious stimulus. n = 9; p < 0.0001, paired Student's t test.

(E) CFA treatment induces a greater aversive response to the noxious stimulus. n = 9; p = 0.0034, paired Student's t test. A CPA score was calculated by subtracting the time rats spent in the PP-paired chamber at the preconditioning phase from the testing phase. A higher CPA score indicates greater pain aversion.

(F) Two days after saline (control) treatment, CFA rats continued to demonstrate increased pain aversion. n = 9; $p < 0.0001$, paired Student's t test.
(G) Two days after ketamine treatment, CFA rats did not show any avoidance for the PP-paired chamber. n = 9; $p = 0.1800$, paired Student's t test.
(H) A single dose of ketamine inhibited the aversive response to acute noxious stimuli in CFA-treated rats for at least 2 days. n = 9; $p < 0.0001$, unpaired Student's t test.
(I) Five days after saline (control) treatment, CFA rats continued to demonstrate increased pain aversion. n = 9; $p < 0.0001$, paired Student's t test.
(J) Five days after ketamine treatment, CFA rats did not show any avoidance for the PP-paired chamber. n = 9; $p = 0.0139$, paired Student's t test.
(K) A single dose of ketamine decreased the aversive response to acute noxious stimuli in CFA-treated rats for at least 5 days. n = 9; $p = 0.0309$, unpaired Student's t test.
Data represented as mean ± SEM.

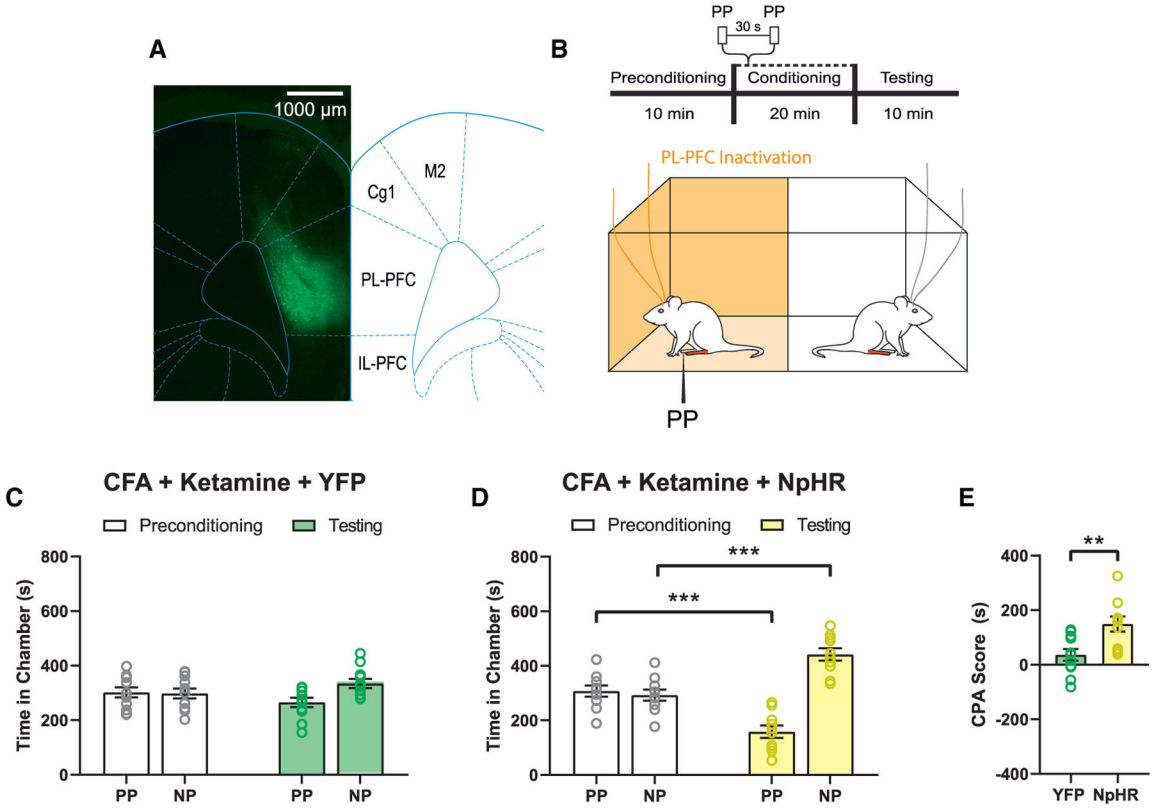

Figure 6. Inactivation of the basal activity of the PL-PFC blocks the anti-aversive effects of ketamine

(A) Localized expression of NpHR-YFP in the pyramidal neurons of the PL-PFC. Scale bar, 1,000 μm.

(B) Schematic of the CPA assay. During conditioning, one of the chambers was paired with PP and laser treatment of the PL-PFC, the other chamber was not.

(C) YFP-treated (control) rats that received CFA and subsequent ketamine treatment did not show any preference or avoidance of either chamber. n = 11; p = 0.1220, paired Student's t test.

(D) Optogenetic inactivation of NpHR-treated rats that received CFA and ketamine treatments showed increased aversion to the PP-paired chamber. n = 10; p = 0.0004, paired Student's t test.

(E) Inactivation of the PL-PFC removes the anti-aversive effects of ketamine treatment. n = 10–11; p = 0.0041, unpaired Student's t test. Data represented as mean ± SEM.

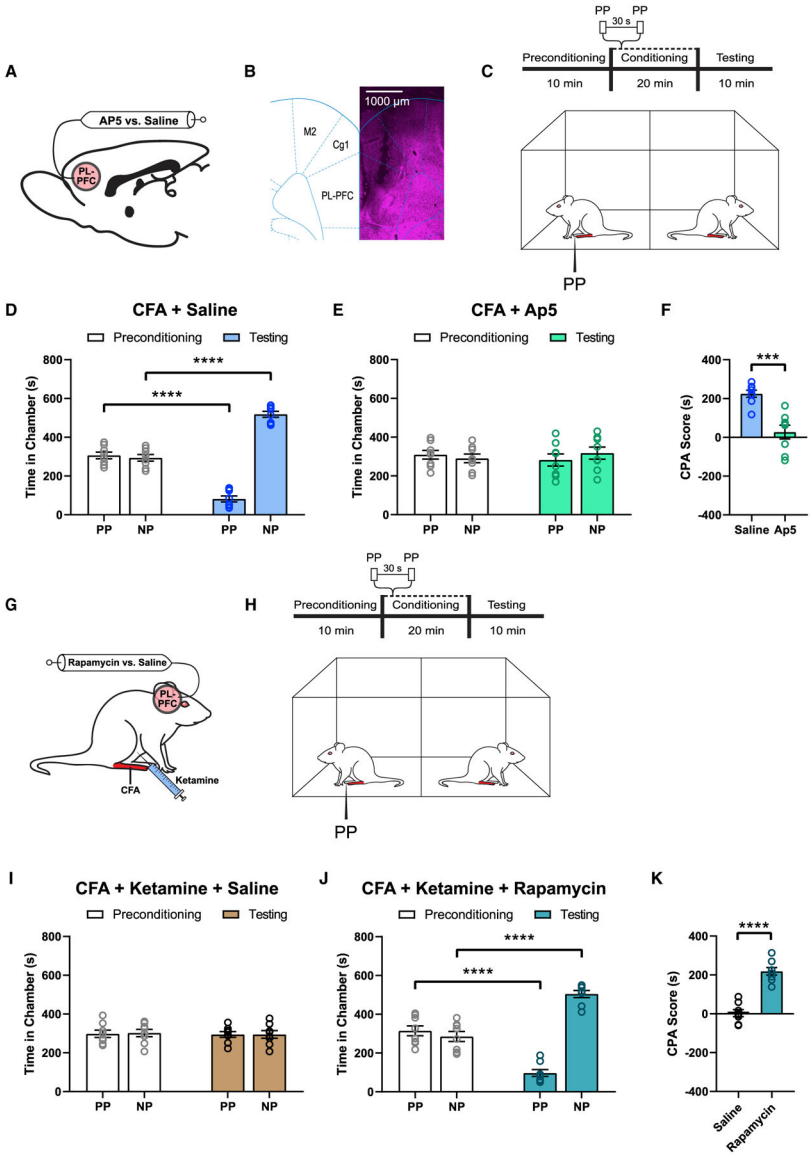

Figure 7. PL-PFC mediates the anti-aversive effects of ketamine

(A) Schematic of intra-PL-PFC drug infusion of AP5 (antagonist of NMDA receptors) versus saline (control).

(B) Representative brain slice indicating the intracranial infusion site in the PL-PFC. Scale bar, 1,000 μm.

(C) Schematic of the CPA assay.

(D) Intra-PL-PFC administration of saline did not alter the aversive response to acute pain in CFA-treated rats. n = 8; $p < 0.0001$, paired Student's t test.

(E) AP5 in the PL-PFC removed the avoidance of PP-paired chamber in CFA-treated rats. n = 8; $p = 0.4692$, paired Student's t test.

(F) AP5 in the PL-PFC removed pain aversion in CFA-treated rats. n = 8; $p = 0.0002$, unpaired Student's t test.

(G) Schematic of intra-PL-PFC drug infusion of rapamycin (translational inhibitor) versus saline (control) prior to ketamine treatment in CFA-treated rats.
(H) Schematic of the CPA assay.
(I) Intra-PL-PFC administration of saline showed no avoidance of the PP-paired chamber after ketamine treatment in CFA-treated rats. $n = 8$; $p = 0.8595$, paired Student's t test.
(J) Intra-PL-PFC administration of rapamycin restored the avoidance of the PP-chamber despite ketamine treatment in CFA-treated rats. $n = 8$; $p < 0.0001$, paired Student's t test.
(K) Pre-treatment of rapamycin in the PL-PFC blocked the anti-aversive effect of ketamine in CFA-treated rats. $n = 8$; $p < 0.0001$, unpaired Student's t test.
Data represented as mean ± SEM.

KEY RESOURCES TABLE

REAGENT or RESOURCE	SOURCE	IDENTIFIER
Bacterial and virus strains		
pENN.AAV1.CamKII.GCaMP6f.WPRE.SV40	Addgene	Cat# 100834-AAV1; RRID: Addgene_100834
pENN.AAV1.CaMKIIa.eNpHR.3.0.EYFP	Addgene	Cat# 26791-AAV1; RRID: Addgene_26971
pENN.AAV1.CamKII(1.3).eYFP.WPRE.hGH	Addgene	Cat# 105622-AAV1; RRID: Addgene_105622
Chemicals, peptides, and recombinant proteins		
Mycobacterium tuberculosis: Complete Freund's Adjuvant	Sigma-Aldrich	Cat# F5881-10ML
Ketamine hydrochloride	Zoetis	N/A
D-(−)-2-Amino-5-phosphonopentanoic acid	Abcam	Cat# ab144482
Rapamycin	Sigma-Aldrich	Cat# R0395-1MG
Experimental models: organisms/strains		
Sprague-Dawley	Taconic Farms	Model SD
Software and algorithms		
MATLAB R2019a	MathWorks	https://www.mathworks.com/products/MATLAB.html
GraphPad Prism 8	GraphPad Software	https://www.graphpad.com/scientific-software/prism/
Inscopix Data Acquisition Software	Inscopix	https://www.inscopix.com/software-analysis#software_idas
Inscopix Data Processing Software	Inscopix	https://www.inscopix.com/software-analysis#software_idps
Constrained Nonnegative Matrix Factorization for microEndoscopic data	Open source	https://github.com/zhoupc/CNMF_E; https://doi.org/10.7554/eLife.28728.001
CellReg	Open source	https://github.com/zivlab/CellReg; Sheintuch et al., 2017
OASIS	Open source	https://github.com/zhoupc/OASIS_matlab; Friedrich et al., 2017
Gephi	Open source	https://gephi.org/
Custom code	This paper	https://doi.org/10.5281/zenodo.5570672
Other		
nVoke 2.0	Inscopix	https://www.inscopix.com/nvoke
Gradient-index lens	Inscopix	https://www.inscopix.com/lenses-viruses
Kwik-Sil Silicone Elastomer	World Precision Instruments	Code KWIK-SIL
Ceramic ferrules	Thorlabs	Cat# CFLC126-10
Compact Power and Energy Meter Console, Digital "4 LCD	Thorlabs	Cat# PM100D
Transistor-transistor logic pulse generator	Doric Lenses	Code OTPG_4
Metabond Quick Adhesive Cement System	C&B	Cat# S380
Fluoromount Aqueous Mounting Medium	Sigma-Aldrich	Cat# F4680-25ML
HC-V550 Camcorder	Panasonic	https://www.panasonic.com/middleeast/en/support/product-archive/camcorder/hc-v550.html